Applied Thermal Engineering 219 (2023) 119639

Contents lists available at ScienceDirect

Applied Thermal Engineering

journal homepage: www.elsevier.com/locate/apthermeng

Research Paper

# Numerical performance of a water source transcritical $CO_2$ heat pump with mechanical subcooling

Fernando Illán-Gómez [a,*], José R. García-Cascales [a], F.J.S. Velasco [a], Ramón A. Otón-Martínez [b]

[a] Departamento de Ingeniería Térmica y de Fluidos, ETSII, Universidad Politécnica de Cartagena. C/ Dr, Fleming s/n 30202, Cartagena, Murcia, Spain
[b] Departamento de Ingeniería y Técnicas Aplicadas, Centro Universitario de la Defensa en la Academia General del Aire, C/ López Peña s/n 30720, San Javier, Murcia, Spain

ARTICLE INFO

*Keywords:*
Water heater
Transcritical cycle
Heat pump
$CO_2$
DMS
IHX

ABSTRACT

In order to improve their efficiency, transcritical $CO_2$ heat pumps need to resort to the use of a subcooling method. Among the different subcooling methods, dedicated mechanical subcooling (DMS) systems and internal heat exchangers (IHX) are currently the more promising technologies. This paper presents a numerical study of a transcritical water source $CO_2$ heat pump during hot water generation using different subcooling methods. Ten different configurations, including both, IHX and DMS, separately and combined in different layouts, some of them not studied previously, are analyzed numerically under the same operating conditions in order to compare their performance. A description of the numerical model is presented: compressors are modeled using the performance curves provided by their manufacturers, expansion valves are modeled as isenthalpic, and heat exchangers are modeled by deriving correlations for the evaporation/condensation pressure and heat transfer rate obtained using a 1D cell-by-cell discretization method previously applied to all heat exchangers. Results are presented for different water heating conditions and show that in most configurations analyzed, the use of a DMS does not improve the performance of the system compared to the base system with IHX. There is only an improvement in the efficiency for two of the configurations analyzed, those in which the main $CO_2$ cycle and the DMS cycle are coupled by the water flowing first through the evaporator of the auxiliary cycle and then through the gas cooler of the main cycle. Specifically, compared to the base cycle with IHX, the configuration that provides the best results (Conf. F* according to the nomenclature used in this work) gives average improvements of around 26% in efficiency and almost 160% in the heating capacity, while the optimum gas cooler pressure is reduced by an average of 12%. Even more, compared to the best performance system previously studied by other authors (indirect DMS without IHX, Conf. F in this work) this configuration improves the efficiency by almost 8.5%, with a decrease in the total capacity lower than 1% and similar gas cooler pressure. The results also show that the auxiliary compressor capacity and the way in which the water is distributed among the main and the auxiliary cycle have an important influence on the efficiency of the system, although that influence depends on the configuration studied. For the configuration that provides the best efficiency (Conf. F*), the optimum efficiency is obtained when the auxiliary compressor capacity is similar to the capacity of the main compressor (55% of the total heating capacity comes from the auxiliary cycle), and the water is mostly heated in the auxiliary cycle (85% of the water flow heated in the condenser of the auxiliary cycle, 15% heated in the gas cooler of the main cycle).

## 1. Introduction

Transcritical $CO_2$ heat pumps are currently improving their penetration in the market of hot water generation, especially in the building sector. Apart from other factors, this can be explained because of the properties of $CO_2$ as a refrigerant (A1 type, natural, cheap, and with a global warming potential (GWP) of 1) and, the high coefficient of performance (COP) obtained, especially when the inlet water temperature is low [1,2]. However, as the inlet temperature of the water to be heated increases, the COP of the system decreases. This is due to the fact that these systems usually use a water-refrigerant heat exchanger working

* Corresponding author.
*E-mail addresses:* fernando.illan@upct.es (F. Illán-Gómez), jr.garcia@upct.es (J.R. García-Cascales), fjavier.sanchez@upct.es (F.J.S. Velasco), ramon.oton@cud.upct.es (R.A. Otón-Martínez).

https://doi.org/10.1016/j.applthermaleng.2022.119639
Received 29 July 2022; Received in revised form 5 November 2022; Accepted 10 November 2022
Available online 14 November 2022

**Nomenclature**

*Acronyms*

| | |
|---|---|
| 3WV | Three-way valve |
| BPV | Back-pressure valve |
| COP | Coefficient of performance |
| DMS | Dedicated mechanical subcooling |
| DHW | Domestic hot water |
| EEV | Electronic expansion valve |
| GWP | Global warming potential |
| IHX | Internal heat exchanger |
| MARD | Mean absolute relative difference |
| SC | Subcoolingdegree |
| SH | Superheating degree |
| TTS | Thermoelectric subcooling system |

*Variables*

| | |
|---|---|
| $A$ | Heat exchange area ($m^2$) |
| $h$ | Specific enthalpy ($kJ \cdot kg^{-1}$) |
| $k_v$ | Flow coefficient ($m^3 \cdot h^{-1}$) |
| $\dot{m}$ | Mass flow rate ($kg \cdot s^{-1}$) |
| $p$ | Pressure (bar) |
| $\dot{Q}$ | Heating capacity (kW) |
| $T$ | Temperature (°C) |
| $v$ | Compressor speed (rpm) |
| $\dot{V}$ | Volumetric flow rate ($m^3 \cdot h^{-1}$) |
| $\dot{W}$ | Compressor power input (kW) |

*Greek*

| | |
|---|---|
| $\Delta$ | Difference (-) |
| $\rho$ | Density ($kg \cdot m^{-3}$) |

*Subscripts*

| | |
|---|---|
| a | Actual operating conditions |
| c | Condenser |
| comp | Compressor |
| e | Evaporator |
| gc | Gas cooler |
| in | Inlet |
| out | Outlet |
| r | Refrigerant |
| rat | Rated conditions |
| s | System |
| t | Total |
| w | Water |

under counter-flow conditions as a gas cooler and, as the inlet water temperature increases, the enthalpy of the refrigerant ($CO_2$) at the outlet of the gas cooler also increases [3,4]. This limits the specific heat absorbed at the evaporator and, consequently, also the specific heat transferred at the gas cooler and the overall COP.

In order to overcome this handicap, transcritical $CO_2$ systems usually resort to the use of a subcooling or after-cooling[1] method, which allows reducing the enthalpy of the refrigerant at the gas cooler outlet and thus improving the efficiency of the system. Typically, the subcooling effect has been obtained by internal methods. Although there are several internal methods that can improve the efficiency of the system, like the use of an economizer or subcooler, or the use of integrated mechanical subcooling [6], the method most frequently used consist of the use of an internal heat exchanger (IHX). As summarized by Llopis et al. [6], the use of an IHX located both in the classical or in non-classical positions, or combined with other methods (combined with ejectors, combined with expanders, or combined with vapor extraction from the intermediate vessel) has been extensively studied by different authors as a way to improve the performance of refrigeration plants. Regarding its use in heat pump systems, although according to White et al. [7], in high-temperature heating applications it is preferable to eliminate the IHX in favor of a larger gas cooler, most authors reported improvements in the performance of the systems studied when an IHX is used. Kim et al. [8] pointed out that the use of an IHX reduces the optimal pressure and improves the COP up to certain discharge pressure. The existence of a limit discharge pressure below which the IHX improves the cycle performance was also reported by other authors [9–11], although [9] and [10] circumscribe that improvement to conditions of high temperature of the refrigerant leaving the gas cooler or the water entering the gas cooler. Although, similarly to what was previously reported in refrigerant plants by Torrella et al. [12], according to Jiang et al. [13] or Cao et al. [14], in heat pump facilities the use of an IHX can also be related, under certain operating conditions, to excessive compressor discharge temperature. According to Illán-Gómez et al. [4], unsafe temperatures can be avoided using an appropriate control system that acts opening the valve that controls the gas cooler pressure in order to decrease that pressure when the compressor discharge temperature approximates the limits of the compressor.

A more recent alternative to internal subcooling methods consists of the use of dedicated subcooling systems, that is currently been studied by different authors. Among these dedicated subcooling systems, the most frequent method is based on the use of an auxiliary vapor compression system that produces the subcooling effect in its evaporator; those systems are usually called dedicated mechanical subcooling (DMS) systems. A different and less frequent approach is based on the use of thermoelectric (Peltier) elements as subcooling devices, which are called thermoelectric subcooling systems (TSS). Both approaches are relatively recent improvements that are being studied by different researchers as a method to enhance the efficiency of $CO_2$ transcritical cycles, mainly in refrigeration applications [6].

During the last few years, several authors have studied the feasibility of the use of DMS systems also in heating applications. Yang et al. [15] studied, both, experimentally and theoretically, a combined R134a and transcritical $CO_2$ system, in which the subcooling effect is obtained indirectly by splitting the feed water into two streams. The first stream is directly warmed up in the R134a condenser, whereas the second stream flows into the R134a evaporator, where it is cooled down, and then flows into the $CO_2$ gas cooler where it initially produces a subcooling effect, improving the efficiency of the $CO_2$ system and then is heated up and mixed with the first stream. The system studied was an air-to-water heat pump, working at ambient temperatures ranging from −20 °C to 7 °C. According to the authors, the system proposed allows reaching an increase in the overall efficiency by up to 22% compared to a standard transcritical $CO_2$ system. The system has been further studied by the authors [16–19] in order to determine the optimal discharge pressure and the optimal intermediate temperature.

Dai et al. have published different papers in which they have numerically studied DMS systems from different perspectives and using R1234yf as refrigerant in the auxiliary cycle [20–24]. In [20,21] they

[1] As pointed out by Mohammadi [5], above the critical pressure there is no real subcooling and therefore the term “subcooling” should not be used. Despite the authors acknowledging that, from a thermodynamic point of view, it would be more appropriate to use the term “after-cooling”, the term “subcooling” is widely used in most of the published research work dealing with transcritical refrigeration and heat pump systems and this work will follow that nomenclature.

study a transcritical reversible air source $CO_2$ heat pump air conditioning system with and without DMS, reporting improvements in both, the COP and the exergy efficiency when the DMS is used. Similar conclusions are obtained in [22,23], in which they compare a transcritical air source $CO_2$ heat pump with a similar system using direct DMS. In [24] they extended the comparison to six different configurations of transcritical air source $CO_2$ heat pumps: a base single-stage transcritical $CO_2$ system, a double-stage transcritical $CO_2$ system with vapor injection, a cascade $CO_2$ system, an indirect DMS system similar to the one proposed in [15], a direct DMS system coupled to a single-stage transcritical $CO_2$ system, similar to that previously studied in [22,23], and a direct DMS system coupled to a double-stage transcritical $CO_2$ system with vapor injection (what they called VIDMS system). They conclude that the VIDMS system was the one that provides the highest efficiency in the whole range of ambient temperatures, from −30 °C to 20 °C. They also have published other papers devoted to refrigeration facilities, obtaining certain conclusions that could probably be extrapolated to heat pump systems. In [25] they studied the influence of the fluid used in the auxiliary DMS cycle, concluding that the mixtures with proper temperature glide are preferable to pure substances. In [26] they compared a single-stage transcritical $CO_2$ refrigeration system with direct DMS that uses R290 as the refrigerant (what they called SMS) with four different configurations of a two-stage transcritical $CO_2$ refrigeration system with direct DMS. Depending on the amount of $CO_2$ that passes through the first throttling valve before entering the intermediate liquid receiver, and on the relative position of the DMS cycle (high or low-pressure side of the main $CO_2$ cycle) four different combinations can be found. When only a part of the $CO_2$ flows through the first throttling valve, the intermediate liquid receiver includes a heat exchanger in which the high-pressure fluid is subcooled by exchanging energy with the bi-phasic fluid at an intermediate pressure, which evaporates before mixing with the fluid that leaves from the low-pressure compressor discharge port. Using those configurations (OTLMS for the low-pressure DMS and OTHMS for the high-pressure DMS according to the nomenclature used by the authors), two different subcooling effects are obtained, the one in the DMS evaporator and the one in the intermediate liquid receiver, which up to a certain point, can be considered similar to what can be found in an IHX. When all the $CO_2$ passes through the first throttling valve (TTLMS for the low-pressure DMS and TTHMS for the high-pressure DMS), the intermediate liquid receiver acts only as a flash tank; the saturated vapor leaving the tank mixes with the superheated vapor leaving the low-pressure compressor and the saturated liquid goes to the $CO_2$ evaporator, and only a subccoling effect is obtained. The results obtained were compared to similar cycles without DMS and, according to the results presented by the authors, the use of DMS improves the COP of the four configurations studied. Regarding the exergy efficiency and the COP of the four two-stage DMS cycles, it seems that at ambient temperatures above 25 °C it is preferable to place the DMS on the high-pressure side of the main cycle and to operate with all $CO_2$ passing through the first throttling valve, although the relative location of the DMS has a stronger impact than the amount of $CO_2$ passing through the first throttling valve and thus the higher exergy efficiency is found for the TTHMS, then the OTHMS, then the TTLMS and the lower values are obtained using the OTLMS. When the ambient temperature is below 20 °C, the differences are less clear; it seems that the COP improves placing the DMS on the low-pressure side of the main cycle, but the exergy efficiency does not follow exactly the same pattern.

Cheng et al. [27] and He et al. [28] also studied different configurations for air source heat pumps. In [27] they proposed a system that is able to switch between a transcritical $CO_2$ cycle with DMS using R1234yf as a refrigerant, and a cascade system formed by a subcritical $CO_2$ cycle on the low-pressure side and a conventional (subcritical) R1234yf cycle on the high-pressure side. To switch between both modes, the heat exchanger that acts as a gas cooler on the transcritical cycle, acts as a desuperheater on the cascade cycle, whereas the R1234yf cycle evaporator acts as a $CO_2$ subcooler in the transcritical cycle and as a $CO_2$ condenser in the subcritical cycle. The authors studied numerically the behavior of the system under six different Chinese climates, with ambient temperatures ranging from −30 °C to 10 °C. They reported COP improvements of 8.7% and 19.4% compared to a conventional transcritical $CO_2$ system with DMS, and a cascade system respectively. In [28] they studied the influence that the water flow configuration has on a transcritical $CO_2$ system with DMS with ambient temperatures ranging from −25 °C to 15 °C. They numerically compared three different water flow configurations. In the first configuration, the water flow is separated into two parallel streams, one flowing through the DMS cycle condenser, and the other flowing through the $CO_2$ gas cooler. In the second one, all the water passes first through the condenser of the DMS cycle and then through the gas cooler. The last configuration studied includes an additional gas cooler; all the water flows initially through a first $CO_2$ gas cooler, then through the condenser of the DMS system, and, finally, through a second $CO_2$ gas cooler. According to the authors, the two gas coolers system can improve the COP of the system by between 3% and 7.6%, depending on the water return/supply temperature.

Although different authors have studied the use of DMS systems in transcritical $CO_2$ systems during hot water generation, it is still necessary to continue researching this subject. To the authors' knowledge, all studies published are devoted to air source heat pumps, which typically present lower evaporation pressure than the water to water heat pumps that will be studied in this work, including ground source or greywater source heat pumps.

Additionally, different papers analyze distinct configurations under different operating conditions, therefore the results obtained by those authors are not directly comparable, and the differences among the configurations proposed are not enough clear. This paper will try to clarify the differences among the different configurations studied by different authors by comparing them under the same operating conditions, as well as to include in the study some configurations not analyzed previously. Even more, in most cases, the comparisons are made against a base cycle that does not include any subcooling method. Since the use of an IHX is an easy way to improve the efficiency of transcritical systems, which has been extensively used by different authors, it seems reasonable to compare a DMS system not only to a base cycle but also to an improved cycle including IHX. This paper will take as the base cycle for comparison a transcritical system that already includes an IHX.

Moreover, most of the papers available in the open literature do not consider the combination of more than one subcooling method, and the few existing papers that analyze the combination of more than one subcooling method are devoted to refrigeration applications: Casi et al. [29] studied the combination of IHX and TSS in a refrigeration facility; the use of double IHX has also been studied both numerically [30] and experimentally [31] by different authors; as previously cited, Liu et al. [26] studied different DMS systems, including a combination of DMS and an intermediate liquid receiver with an incorporated heat exchanger which, in a certain way can be considered to act as a subcooling system. To the best of the authors' knowledge, those are the more representative papers in the open literature that analyze the combination of more than one subcooling method, and all of them are devoted to refrigeration systems. Therefore, further efforts are necessary to study the combination of DMS and IHX in the same heat pump system.

This work seeks to evaluate whether the use of a DMS system coupled to a transcritical $CO_2$ heat pump cycle can improve the overall performance of the coupled system and what are the operational parameters that optimize the system. Thus, this paper presents a numerical study of the use of a DMS system using R1234yf as refrigerant, during hot water generation in a water source transcritical $CO_2$ heat pump under different working conditions and different water flow configurations. The results obtained will be compared to those obtained in a base cycle that includes an alternative subcooling system, namely an IHX. Even more, this paper will analyze whether the use of two subcooling methods (IHX and DMS) combined in the same system is able to improve its performance.

The paper is structured as follows: the following section describes the

model developed in MATLAB. That section also describes the different operating conditions that have been introduced to the model in order to study the influence of the DMS system on the performance of the heat pump. The third section describes the results of the comparison of the different systems and water flow configurations that have been compared for the transcritical $CO_2$ cycle. Finally, the last section summarizes the main conclusions drawn.

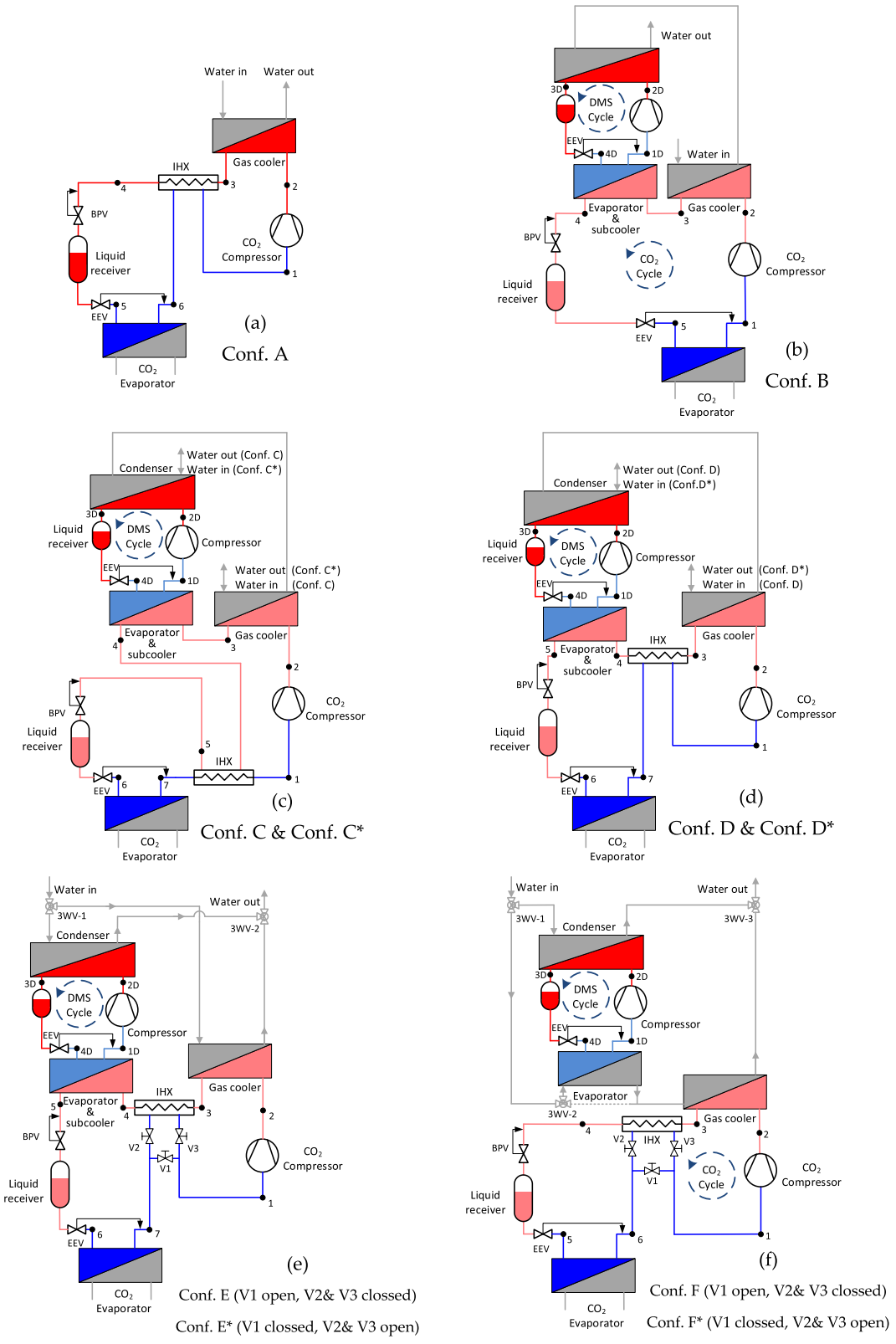


**Fig. 1.** $CO_2$-DMS configurations analyzed for hot water generation.

## 2. Systems studied

Fig. 1 shows the different configurations studied in this work for hot water generation.

Conf. A is the base $CO_2$ cycle with IHX and without DMS. This configuration is taken as a reference to evaluate the interest in employing a DMS system and corresponds to the one previously studied by the authors in previous works [3,4,32,33]. The numerical model used for this configuration has been already validated under different operating both in stationary and transient conditions [3,4,32,33].

Conf. B represents a $CO_2$ cycle with DMS and without IHX. Different authors have studied this configuration as a way to improve the efficiency of transcritical $CO_2$ refrigeration plants. According to Llopis et al. [6], the improvement reported using a DMS (up to 28.8% or even up to 67.7% when used jointly with an expander) is higher than the improvement obtained with an IHX (up to 20%, but not recommended with expansion energy recovery elements). The same or very similar design has been studied by several authors in heating applications [24,28] although, in most cases, those studies do not include a comparison with a basic cycle with IHX. Wang&Zhang [34] performed that comparison and, according to their results, the use of an IHX as subcooling method provides higher efficiency than the use of a DMS system when heating water from 50 °C to 70 °C at ambient temperatures ranging from −25 °C to 45 °C.

Conf. C, Conf. D, Conf. E, and Conf. F represent different variations of a $CO_2$ cycle with DMS and IHX. To the best of the authors' knowledge, the combination of those two subcooling methods in the same system has not been previously studied.

The difference between Conf. C and Conf. D lies in the relative position of the IHX and the DMS system. In Conf. C, the DMS evaporator-$CO_2$ subcooler is located before the IHX, whereas in Conf. D the IHX is placed before the DMS system. When the $CO_2$ passes first through the IHX, the superheating obtained in the low-pressure side of the IHX increases, and the efficiency of the $CO_2$ system operating as a heat pump is expected to improve, whereas the evaporation temperature of the DMS cycle will decrease and thus the efficiency of the DMS cycle is expected to worsen. On the other hand, when the $CO_2$ flows first through the DMS evaporator, the effect is the opposite, DMS evaporation temperature will increase improving the DMS cycle efficiency and the superheating degree at the IHX low-pressure side outlet will decrease, degrading the efficiency of the $CO_2$ cycle. The difference between Conf. C and Conf. D, and Conf. C* and Conf. D* is the water flow circulation order. In Conf. C and Conf. D, the water passes first through the gas cooler and then through the condenser, whereas in Conf. C* and Conf. D* the water flow is reversed. When the water passes first through the $CO_2$ gas cooler, the optimal pressure of the $CO_2$ cycle decreases, and its efficiency increases, but the water enters the DMS cycle condenser at a higher temperature, and therefore the DMS cycle condensing temperature increases, and its efficiency decreases. When the water flow is reversed, the DMS cycle operates at a lower condensing temperature (the efficiency increases) but the $CO_2$ cycle operates at higher optimal pressure (the efficiency decreases). Those four configurations have been included here to study which effect dominates and provides the best overall performance.

Conf. E corresponds in Fig. 1.e to the situation in which valve V1 is open, and valves V2 and V3 are closed. It is similar to Conf. B, but the water flow is divided into two different streams, one sent to the condenser of the auxiliary cycle and the other sent to the gas cooler of the main cycle. Therefore, as in Conf. B, the system operates without IHX, but by dividing the water flow into two streams, it is expected to not penalize the efficiency of one cycle over the other. This configuration is similar to the layout that Dai et al. [24] called direct dedicated mechanical subcooling (DDMS), and Cheng et al. [27] simply called transcritical $CO_2$ heat pump with DMS. It has been included in this study to compare its performance with the other designs studied, and as a base cycle in which an IHX can be also included in order to analyze its ability to improve the overall efficiency of this configuration. That case corresponds to Conf. E*, in which valve V1 is closed, and valves V2 and V3 are open, and therefore the system operates with a combination of two subcooling methods, DMS and IHX.

Conf. F represents a $CO_2$ cycle without IHX (valve V1 open, valves V2&V3 closed in Fig. 1.f), and an auxiliary subcooling cycle. In this design the water flow is divided into two streams, one flows through to the condenser of the auxiliary cycle, and the other one passes first through the evaporator of the auxiliary cycle and then is sent to the gas cooler of the main cycle. This layout is similar to that extensively studied by Yang et al. [15] and Song et al. [16–19], and also by Dai et al. [24], who called it indirect dedicated mechanical subcooling (IDMS). Finally, Conf. F* represents a similar design but includes an IHX (valve V1 closed, valves V2&V3 open in Fig. 1.f).

As pointed out in previous paragraphs, some of these configurations have been already studied by other authors, but have been included here in order to compare them under the same operating conditions. Additionally, the combination of two different subcooling methods (DMS and IHX) has not been considered by most of the previous researchers and therefore has been included here in order to assess its ability to improve the efficiency compare to each of those subcooling methods separately.

For better clarity, the temperature-entropy diagrams for several representative configurations can be seen in Fig. 4, jointly with an explanation of the differences among them in section 4.1.

## 3. Numerical model

In order to enhance the efficiency of the overall system, a fundamental design condition when a DMS cycle is considered to be coupled to a base cycle (such as the case here with the transcritical $CO_2$ cycle), is that the COP of the coupled cycle (i.e., base $CO_2$ main cycle combined to DMS cycle) must be greater than the COP of the base cycle (i.e., $CO_2$ cycle). This and other conditions were evaluated for the coupled system under different working conditions in order to evaluate if the introduction of the DMS cycle improves the overall performance of the system. In this work, the global COP of the facility is defined as:

$$COP = \frac{\dot{Q}_{gc} + \dot{Q}_c}{\dot{W}_{CO_2} + \dot{W}_{R1234yf}} \tag{1}$$

where $\dot{Q}_{gc}$ is the heating capacity at the gas cooler of the main cycle, $\dot{Q}_c$ is the heating capacity at the condenser of the DMS cycle, and $\dot{W}_{CO_2}$ and $\dot{W}_{R1234yf}$ are the power inputs at the $CO_2$ and R1234yf compressors. It has to be taken into account that the refrigerant flow rate at the R1234yf cycle can vary depending on the working conditions, and it can be estimated as:

$$\dot{m}_{R1234yf} = \dot{m}_{CO2}\hat{A}\cdot\frac{\Delta h_{CO2}}{\Delta h_{R1234yf}} \tag{2}$$

where $\Delta h_{CO2}$ and $\Delta h_{R1234yf}$ are the enthalpy change of $CO_2$ and R1234yf at the heat exchanger acting as $CO_2$ cycle subcooler and R1234yf cycle evaporator.

All main components of both, the auxiliary and the main cycle, have been modeled and included in a numerical model of the coupled system. The components of the main cycle included in the model are those that actually form part of the experimental facility described in previous works [3,4,32,33]. The components of the auxiliary R1234yf cycle have been selected using their respective manufacturer's selection software in order to design an auxiliary cycle that can be coupled to the existing main cycle. In this way, those configurations that are more promising according to the results provided by the numerical study developed here can be studied in future experimental works. Table 1 summarizes the main characteristics of those components.

The mass flow rate and the power consumption of both compressors have been modeled using a third-degree equation of ten coefficients, according to the ANSI/ARHI Standard 540–2015 [35].

**Table 1**
Main components of the cycle and their characteristics.

| | Equipment | Manufacturer | Model | Technical info |
|---|---|---|---|---|
| $CO_2$ cycle | Evaporator | Swep | B8Tx26P | $A = 0.552\ m^2$ |
| | Compressor | Dorin | CD 300H | $\dot{V} = 1.46 m^3 \hat{A} \cdot h^{-1}$ |
| | Gas cooler | Swep | B16x34P | $A = 1.31\ m^2$ |
| | IHX | Swep | B17x4P | $A = 0.082\ m^2$ |
| | BPV | Carel | E2V11 | $k_v = 0.042\ m^3 \cdot h^{-1}$ |
| | EEV | Carel | E2V24 | $k_v = 0.18\ m^3 \cdot h^{-1}$ |
| | Subcooler | Swep | B18Hx20 | $A = 0.738\ m^2$ |
| R1234yf cycle | Evaporator | | | |
| | Compressor | Copeland | YH04K1E | $\dot{V} = 5.76 m^3 \hat{A} \cdot h^{-1}$ |
| | Condenser | Swep | BX8THx16 | $A = 0.322\ m^2$ |
| | EEV | Danfoss | ETS 6–25 | $k_v = 0.164\ m^3 \cdot h^{-1}$ |

Since the $CO_2$ compressor is a transcritical one, those polynomials take the evaporation temperature and the gas cooler pressure as independent variables:

$$x = C_1 + C_2\hat{A}\cdot T_e + C_3\hat{A}\cdot p_{gc} + C_4\hat{A}\cdot T_e^2 + C_5\hat{A}\cdot T_e\hat{A}\cdot p_{gc} + C_6\hat{A}\cdot p_{gc}^2 + C_7\hat{A}\cdot T_e^3 + C_8\hat{A}\cdot p_{gc}\hat{A}\cdot T_e^2 + C_9\hat{A}\cdot T_e\hat{A}\cdot p_{gc}^2 + C_{10}\hat{A}\cdot p_{gc}^3 \quad (3)$$

where $x$ is the dependent variable ($\dot{m}_r$ or $\dot{W}_r$), $T_e$ is the evaporation temperature (in °C), $p_{gc}$ is the gas cooler pressure (in bar), and the adjustment coefficients, $C_i$, depend on the variable considered and can be obtained from Dorin Software [36].

The coefficients are only provided for a superheating degree on 10 K, according to the European Standard EN 12900:2013 [37], so different corrections had been tested in previous works [3], including the Dabiri&Rice correction [38], in order to take into account the decrease in the fluid density when the superheating increases. The final expression used here is an experimentally obtained equation in the form:

$$x = (\rho_a/\rho_{rat})\hat{A}\cdot\left[C_1 + C_2\hat{A}\cdot T_e + C_3\hat{A}\cdot p_{gc} + C_4\hat{A}\cdot T_e^2 + C_5\hat{A}\cdot T_e\hat{A}\cdot p_{gc} + C_6\hat{A}\cdot p_{gc}^2 + C_7\hat{A}\cdot T_e^3 + C_8\hat{A}\cdot p_{gc}\hat{A}\cdot T_e^2 + C_9\hat{A}\cdot T_e\hat{A}\cdot p_{gc}^2 + C_{10}\hat{A}\cdot p_{gc}^3\right] \quad (4)$$

where the adjustment coefficients, $C_i$, are not those provided by the manufacturer but calculated by polynomial regression to more than 6000 experimental points obtained during transient conditions with gas cooler pressure ranging from 50 to 111 bar and water temperature at the inlet of the evaporator ranging from 5 to 20 °C [32]. Fig. 2 shows the adjustment obtained, with the values of the mean absolute relative difference (MARD), and the values of the coefficients $C_i$, for both, the mass flow rate, and the compressor power input. Although in general the adjustment is very good, under certain conditions the deviation can reach maximum values of 21.76% for $\dot{W}_r$, and 14.47% for $\dot{m}_r$.

In the case of the R1234yf compressor, the software allows personalizing the superheating degree to obtain the adjustment coefficients. Those coefficients were obtained for a superheating degree of 5 K, which has been assumed constant in all simulations. The final expression is:

$$x = C_1 + C_2\hat{A}\cdot T_e + C_3\hat{A}\cdot T_c + C_4\hat{A}\cdot T_e^2 + C_5\hat{A}\cdot T_e\hat{A}\cdot T_c + C_6\hat{A}\cdot T_c^2 + C_7\hat{A}\cdot T_e^3 + C_8\hat{A}\cdot T_c\hat{A}\cdot T_e^2 + C_9\hat{A}\cdot T_e\hat{A}\cdot T_c^2 + C_{10}\hat{A}\cdot T_c^3 \quad (5)$$

where $x$ is the dependent variable ($\dot{m}_r$ or $\dot{W}_r$), $T_e$ and $T_c$ are the evaporation and condensation temperatures (in °C), and the adjustment coefficients, $C_i$, depend on the variable considered and can be obtained from Copeland Select 8 Software [39] for the desired superheating degree. Since the superheating degree is configurable and this compressor has not been experimentally tested yet, no experimental corrections have been considered.

The numerical model assumes for both compressors that all the energy input is actually turned into useful work that goes to the refrigerant.

Finally, all expansion devices are modeled as isenthalpic, and all heat exchangers have been modeled by deriving correlations for the evaporation/condensation pressure and heat transfer rate.

In order to obtain the correlations that describe the behavior of each heat exchanger, two different approaches have been used. The approach used to model all the heat exchangers of the main $CO_2$ cycle is the same used in previous works [4,33]. It consists of a 1D cell-by-cell discretization method that divides the heat exchanger into $n$ cells, applies the energy conservation equation to each cell, and solves iteratively until convergence in the heat transfer area is reached; further details of this method can be found in [33]. On the other hand, since the condenser of the auxiliary R1234yf cycle is a conventional water/subcritical refrigerant plate heat exchanger, a well-known commercial software, IMST-ART [40], extensively used by several authors in their research work [41–46] as a simulation tool to model refrigeration cycle components, including different types of heat exchangers, has been used to obtain condensation pressure and heat transfer rate. The same method has been used to model the evaporator of the auxiliary cycle for Conf. F&F*, which also operates as a conventional water/subcritical refrigerant plate heat exchanger.

The procedure used to obtain the correlations consist of modeling each heat exchanger as an independent element that operates under a set of 19,500 different realistic conditions taken as input for the model. Although the specific input values depend on the heat exchanger considered, the method is the same for all of them. Table 2 summarizes the process followed to obtain the inputs for both, the evaporator and the gas cooler of the main $CO_2$ cycle.

In both heat exchangers, the water inlet temperature and mass flow rate are taken as inputs of the model, as well as the pressure in the gas cooler, which can be controlled by a back-pressure valve (BPV). The refrigerant mass flow rate is calculated from the evaporation temperature, gas cooler pressure, and superheating, using eq. (5). Although in the case of the evaporator, the evaporation pressure is in fact output of

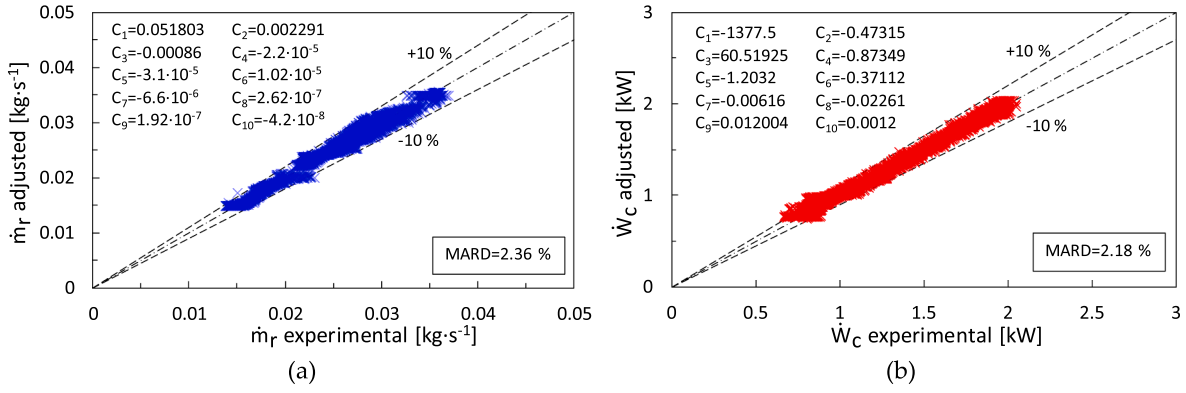


**Fig. 2.** Comparison between experimental and predicted values of mass flow rate and compressor power consumption for the adjustment adopted ($CO_2$ compressor).

**Table 2**
Input parameters used to obtain heat exchanger performance curves.

| | Evaporator | Gas cooler |
|---|---|---|
| Inputs | $T_{w,e,in}, \dot{m}_{w,e,in}, \dot{m}_r, h_{r,e,in}, SH$ | $T_{w,gc,in}, \dot{m}_{w,gc,in}, \dot{m}_r, h_{r,gc,in}, p_{gc}$ |
| Outputs | $p_e$ | $h_{r,gc,out}$ |
| **Model inputs** | | |
| $T_{w,in}$ | 5 data (10–30 °C; $\Delta T$=5 °C) | 5 data (10–50 °C; $\Delta T$=10 °C) |
| $\dot{m}_{w,in}$ | 5 data (0.1–0.5 kg·s$^{-1}$; $\Delta\dot{m}$=0.1 kg·s$^{-1}$) | 5 data (0.05, 0.15, 0.3, 0.6, and 1 kg·s$^{-1}$) |
| $T_e$ | – | 5 data ($T_{w,e,in} - \Delta T_e$) |
| $T_{gc,out}$ | 5 data ($T_{w,gc,in} - \Delta T_{gc}$) | – |
| $p_{gc}$ | 26 data (70–120 bar; $\Delta p$=2 bar) | |
| $SH$ | 2 data (5&10 K) | |
| $SH$ in IHX | 3 data (0, 10, and 20 K) | |
| $\dot{m}_r$ | Calculated | |
| $h_{r,in}$ | Calculated | |

the model, as a first approximation and in order to calculate the refrigerant mass flow rate, it is supposed to be known for both, the evaporator and the gas cooler, assuming a certain temperature difference between the water entering the evaporator and the evaporation temperature, which depends on the water mass flow rate, $\Delta T_e = f(\dot{m}_{w,e})$. In the case of the gas cooler, the same process is used to obtain the refrigerant inlet enthalpy from the compressor power input, whereas in the case of the evaporator, that inlet enthalpy is calculated from the gas cooler pressure and the refrigerant temperature at the outlet of the IHX high-pressure side. To obtain the temperature of the refrigerant at the gas cooler outlet, a certain temperature difference between the refrigerant leaving the gas cooler and the water entering the gas cooler was assumed, which again, depends on the water mass flow rate, $\Delta T_{gc} = f(\dot{m}_{w,gc})$. Finally, the temperature at the IHX high-pressure side outlet is obtained from an energy balance in the IHX, assuming a certain efficiency for the IHX.

Once both the evaporator and the gas cooler have been modeled, their outputs (refrigerant mass flow rate and enthalpy at low and high-pressure side outlet) are taken as input to model the IHX.

When all the heat exchangers are properly modeled, they are integrated, jointly with the compressor and the expansion valve in a global model for the whole $CO_2$ transcritical cycle. This model, corresponding to Conf. A, has already been validated with experimental results in previous works [4].

A similar procedure is used to obtain the correlations for the evaporator and the condenser of the R1234yf cycle. When all the components of the DMS system are modeled, they are joined in a model for the global $CO_2$-DMS cycle built up in MATLAB, which is used to obtain the results presented in the following section.

As an example, the flowchart for the numerical model of Conf. E* has been detailed in Fig. 3 and will be explained in detail in the following paragraphs. The enumeration of all points corresponds to the numeration followed in Fig. 1e and Fig. 6e.

1. Start. Read the inputs ($p_{gc}$, $T_{w,s,in}$, $T_{w,s,out}$, $SH$, $T_{w,e,in}$, $\dot{m}_{w,e}$) and assume an initial value for the evaporation pressure of the main $CO_2$ cycle ($p_{e,CO2} = 30$ bar) and the water mass flowrate through the gas cooler ($\dot{m}_{w,gc} = 0.33$ kg·s$^{-1}$).
2. Calculate the main $CO_2$ cycle evaporation temperature ($T_6$) as the saturation temperature corresponding to the evaporation pressure assumed in step 1. Calculate the temperature at the evaporator outlet ($T_7$) by adding the superheating (SH) to $T_6$.
3. For the first iteration of the loop (i = 1), assume that there is no IHX ($h_1 = h_7$). After the first iteration (i greater than 1) take the enthalpy at the compressor inlet ($h_1$) from the previous iteration.
4. Calculate the actual density at the compressor inlet ($\rho_1$), and the rated density, corresponding to a superheating degree of 10 K according to the European Standard EN 12900:2013.
5. Calculate the refrigerant mass flow rate ($\dot{m}_{CO2}$) and the compressor power input ($\dot{W}_{CO2}$) using equation (4), and the adjustment coefficients reported in [3] and obtained from correlation of experimental values.
6. Calculate the enthalpy at the compressor outlet assuming adiabatic and steady-state operation of the compressor: $h_2 = h_1 + \dot{W}_{CO2}/\dot{m}_{CO2}$.
7. Calculate the temperature at the gas cooler outlet ($T_3$) using its performance correlations obtained using the procedure described in previous paragraphs and the values calculated in previous steps or taken as inputs: $T_3 = f(h_2, p_{gc}, \dot{m}_{CO2}, \dot{m}_{w,gc}, T_{w,gc,in})$.
8. Calculate the enthalpy at the gas cooler outlet ($h_3$) from its temperature ($T_3$) and pressure ($p_{gc}$) using REFPROP and neglecting pressure drop in the gas cooler.
9. Calculate the enthalpy at the low-pressure side IHX outlet ($h_1$) using its performance correlations obtained using the procedure described in previous paragraphs and the values calculated in previous steps: $h_1 = f(T_3, T_7, \dot{m}_{CO2})$.
10. Calculate the enthalpy at the high-pressure side IHX outlet ($h_4$) from the IHX energy balance: $h_4 - h_3 = h_7 - h_1$.
11. Start de DMS cycle submodel. Read the inputs ($\dot{m}_{w,c} = \dot{m}_{w,gc}$, $T_{w,c,in} = T_{w,gc,in}$, $SC = 0$, $SH = 5$ K) and assume an initial value for the evaporation and the condensation pressures of the DMS cycle ($p_{e,DMS} = 3$ bar, $p_{c,DMS} = 9$ bar).
12. Calculate the DMS cycle evaporation temperature ($T_{4D}$) and condensation temperature ($T_{4D}$) as the saturation temperatures corresponding to the evaporation and condensation pressures assumed in step 11. Calculate the temperature at the evaporator outlet ($T_{1D}$) by adding the superheating ($SH$) to the evaporation temperature, $T_{4D}$.
13. Calculate the refrigerant mass flow rate ($\dot{m}_D$) and the compressor power input ($\dot{W}_D$) using equation (5) and the adjustment coefficient provided by its manufacturer.
14. Calculate the enthalpy at the four state points. The enthalpy at 1D is calculated from its temperature (step 11) and pressure (initial value assumed at step 11). The enthalpy at 2D is calculated similarly to step 6. The enthalpy at 3D is calculated from its pressure (initial value assumed at step 11) and subcooling given as input in step 11 ($SC = 0$ K). The expansion valve is assumed isenthalpic and therefore $h_{4D} = h_{3D}$.
15. Recalculate the enthalpy at the condenser outlet ($h_{3D^*}$) and the condensing pressure ($p_{c,D^*}$) using the DMS condenser performance correlations obtained according to the procedure described in previous paragraphs and the values calculated in previous steps or taken as inputs: $h_{3D^*} = f(h_{2D}, \dot{m}_D, \dot{m}_{w,c}, T_{w,c,in}, SC)$; $p_{c,D^*} = f(h_{2D}, \dot{m}_D, \dot{m}_{w,c}, T_{w,c,in}, SC)$.
16. Calculate the absolute value of the relative errors in the condenser pressure (error1) and specific heat transfer rate (error2): error1 = abs($(p_{c,D^*} - p_{c,D})/p_{c,D^*}$); error2 = abs{$[(h_{3D^*} - h_{2D}) - (h_{3D} - h_{2D})]/(h_{3D^*} - h_{2D})$}.
17. Assign a new value for the condensing pressure: $p_{c,D} = (p_{c,D^*} + p_{c,D})/2$.
18. Recalculate the enthalpy at the evaporator outlet ($h_{1D^*}$) and the evaporating pressure ($p_{e,D^*}$) using the DMS evaporator performance correlations obtained according to the procedure described in previous paragraphs and the values calculated in previous steps or taken as inputs: $h_{1D^*} = f(h_{4D}, \dot{m}_D, \dot{m}_{CO2}, T_4, h_4, SH)$; $p_{e,D^*} = f(h_{4D}, \dot{m}_D, \dot{m}_{CO2}, T_4, h_4, SH, p_{gc})$.
19. Calculate the absolute value of the relative errors in the evaporator pressure (error3) and specific heat transfer rate (error4): error3 = abs($(p_{e,D^*} - p_{e,D})/p_{e,D^*}$); error4 = abs{$[(h_{1D^*} - h_{4D}) - (h_{1D} - h_{4D})]/(h_{1D^*} - h_{4D})$}.
20. Assign a new value for the evaporating pressure: $p_{e,D} = (p_{e,D^*} + p_{e,D})/2$.
21. Calculate the error for the DMS cycle (errorDMS) as the maximum value of the four errors calculated in steps 16 and 19.

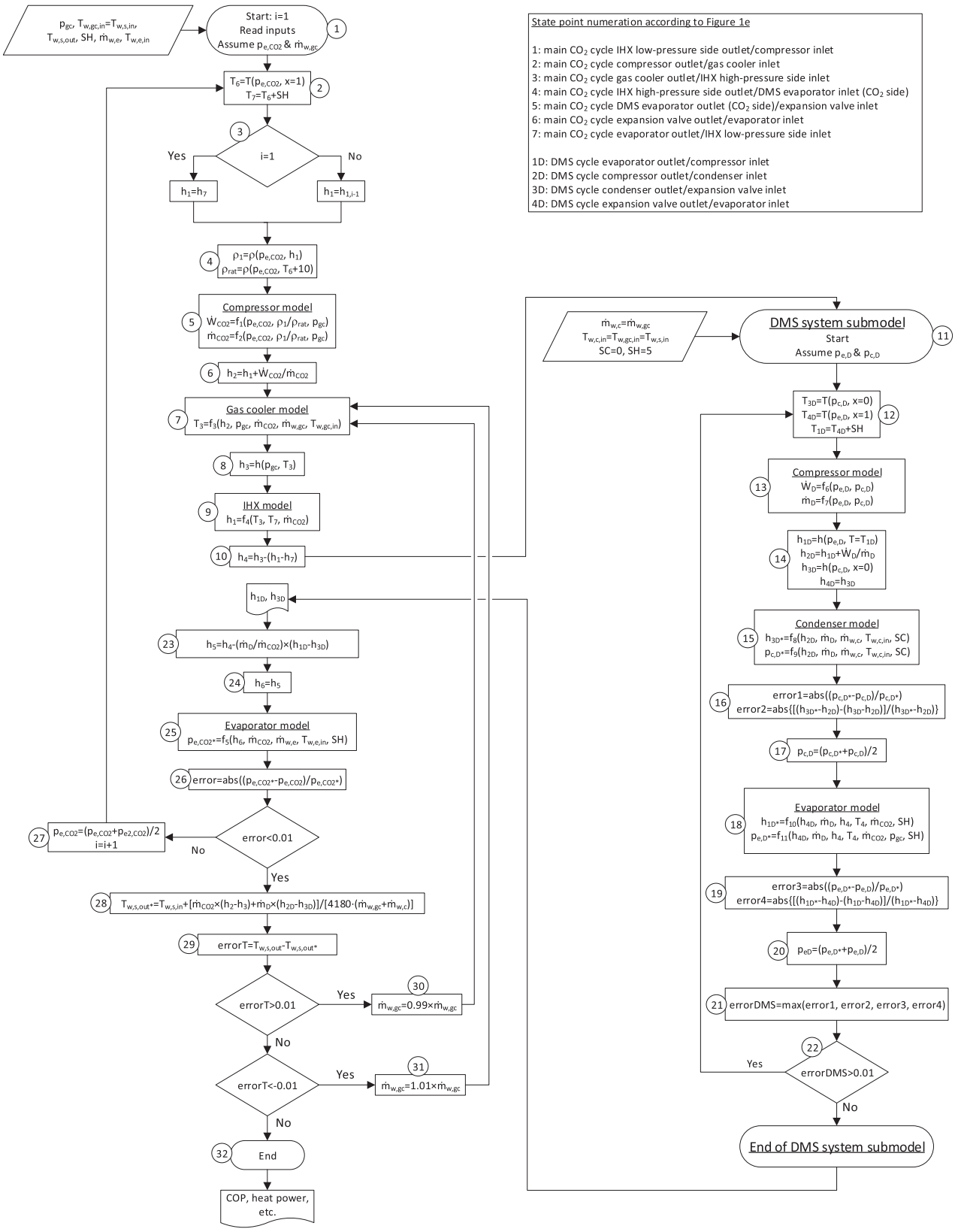


**Fig. 3.** Flowchart for Conf. E*.

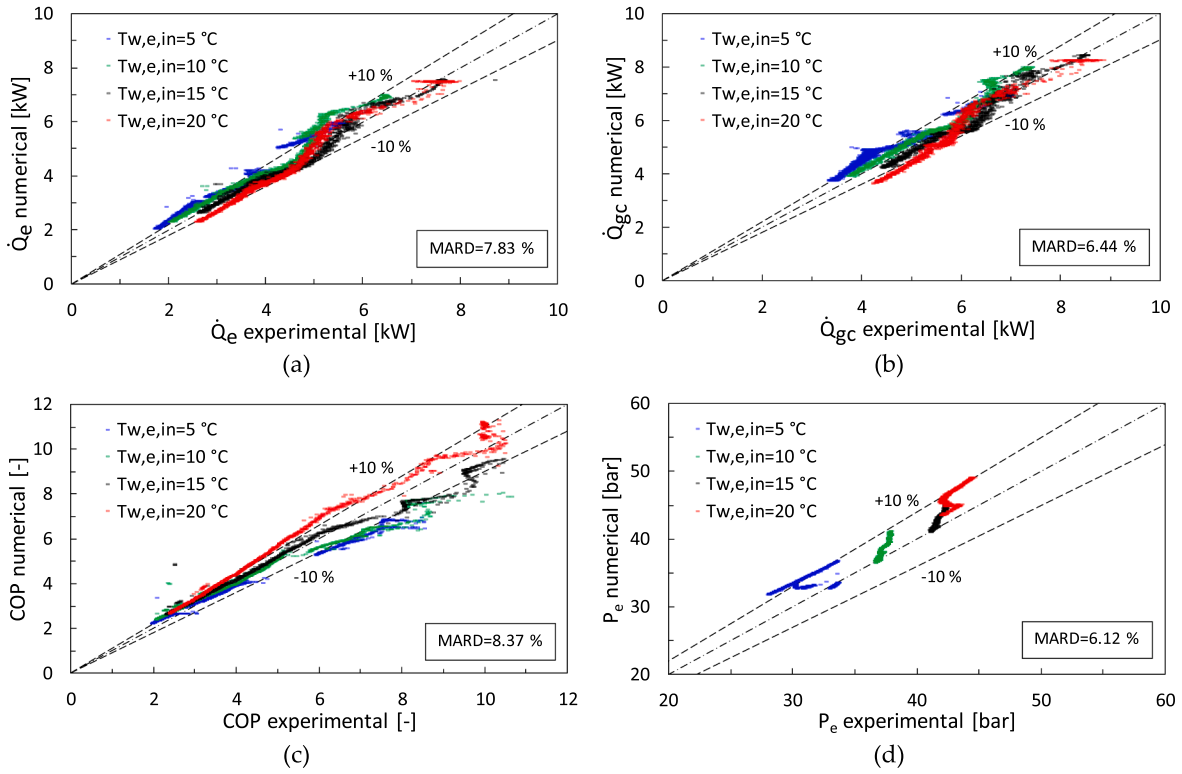


**Fig. 4.** Model validation for Conf. A. Comparison between experimental and numerical results for the evaporator heat transfer rate (a), gas cooler heat transfer rate (b), COP (c), and evaporation pressure (d).

22. If the maximum error among evaporation and condensation pressure, and specific heat transfer rate at the evaporator and the condenser is below 1%, end the DMS cycle submodel and continue with the main cycle submodel, taking $h_{1D}$ and $h_{3D}$ as outputs of the DMS cycle submodel. If not, return to step 12 using the new condensing and evaporating pressures calculated in steps 17 and 20.
23. Calculate the enthalpy of the $CO_2$ leaving the evaporator of the DMS cycle/subcooler of the $CO_2$ cycle ($h_5$) from the energy balance of the heat exchanger: $\dot{m}_{CO2}\cdot(h_4-h_5)=\dot{m}_D\cdot(h_{1D}-h_{3D})$.
24. Calculate the enthalpy at the evaporator inlet assuming that the expansion valve is isenthalpic ($h_6 = h_5$).
25. Recalculate the $CO_2$ evaporating pressure ($p_{e,CO2*}$) using the $CO_2$ evaporator performance correlations obtained according to the procedure described in previous paragraphs and the values calculated in previous steps or taken as inputs: $p_{e,CO2*}=f(h_6, \dot{m}_{CO2}, \dot{m}_{w,e}, T_{w,e,in}, SH)$.
26. Calculate the absolute value of the relative error in the evaporator pressure: error = abs$((p_{e,CO2*}-p_{e,CO2})/p_{e,CO2*})$.
27. If the error in the $CO_2$ evaporating pressure is higher than 1%, assign a new value for the $CO_2$ evaporating pressure, $p_{e,CO2}=(p_{e,CO2*}+p_{e,CO2})/2$, make i = i + 1, and return to step 2, otherwise go to step 28.
28. Calculate the temperature of the water leaving the system ($T_{w,s,out*}$) from the energy balance in both, the $CO_2$ gas cooler and the DMS condenser:
    - Gas cooler energy balance: $\dot{m}_{CO2}\cdot(h_2-h_3)=\dot{m}_{w,gc}\cdot4180\cdot(T_{w,gc,out}-T_{w,s,in})$.
    - Condenser energy balance: $\dot{m}_D\cdot(h_{2D}-h_{3D})=\dot{m}_{w,c}\cdot4180\cdot(T_{w,c,out}-T_{w,s,in})$.
    - $\dot{m}_{w,gc}\cdot4180\cdot(T_{w,gc,out}-T_{w,s,in})+\dot{m}_{w,c}\cdot4180\cdot(T_{w,c,out}-T_{w,s,in})=\dot{m}_{w,s}\cdot4180\cdot(T_{w,s,out*}-T_{w,s,in})$
    - $\dot{m}_{w,gc}=\dot{m}_{w,c}\Rightarrow(T_{w,gc,out}-T_{w,s,in})=(T_{w,c,out}-T_{w,s,in})\Rightarrow T_{w,gc,out} = T_{w,c,out} = T_{w,s,out*}$
    - $\dot{m}_{CO2}\cdot(h_2-h_3)+\dot{m}_D\cdot(h_{2D}-h_{3D})=(\dot{m}_{w,gc}+\dot{m}_{w,c})\cdot4180\cdot(T_{w,s,out*}-T_{w,s,in})\Rightarrow$
    - $\Rightarrow T_{w,s,out*}= T_{w,s,in} + [\dot{m}_{CO2}\times(h_2-h_3)+\dot{m}_D\times(h_{2D}-h_{3D})]/[4180\cdot(\dot{m}_{w,gc}+\dot{m}_{w,c})]$
29. Calculate the error in the temperature of the water leaving the system: errorT = $T_{w,s,out}-T_{w,s,out*}$.
30. If the temperature calculated is more than 0.01 °C lower than the desired value (errorT > 0.01), decrease the water mass flow rate a 1% and return to step 7, otherwise go to step 31.
31. If the temperature calculated is more than 0.01 °C higher than the desired value (errorT < 0.01), increase the water mass flow rate a 1% and return to step 7, otherwise go to step 32.
32. Calculate the variables of interest (COP, heat power, etc.) and stop.

In order to validate the method, Fig. 4 shows the comparison of the results obtained for Conf. A using the numerical method presented, against more than 6000 experimental points obtained during transient conditions with gas cooler pressure ranging from 50 to 111 bar and water temperature at the inlet of the evaporator ranging from 5 to 20 °C [32]. The figure includes results for the evaporator heat transfer rate ($\dot{Q}_e$; Fig. 4a), the gas cooler heat transfer rate ($\dot{Q}_{gc}$; Fig. 4b), the efficiency of the system (COP; Fig. 4c), and the evaporation pressure ($P_e$; Fig. 4d). Although there are some points that present deviations over 10%, in most cases the difference between experimental and numerical results is lower than 10%, with MARD values ranging from a minimum value of 6.12% for the evaporation pressure to a maximum of 8.37% for the COP. Numerical results are strongly influenced by the accuracy of the model used to describe the behavior of the compressor. The correlations used to predict the compressor mass flow rate and power input have MARD values of 2.36% and 2.18% respectively, although under certain operating conditions, can reach values higher than 20% for the power input, which could explain the differences shown in Fig. 4.

## 4. Results and discussion

This section presents and discuss the main results obtained using the model described previously.

### 4.1. Influence of the configuration

Fig. 5 shows the relationship between the COP and the gas cooler pressure during hot water generation for space heating at an intermediate temperature according to the EN-14511–2 standard [47], (the gas cooler water inlet/outlet temperatures are 40/45 °C). The results have been obtained for a water temperature of 15 °C at the evaporator inlet, evaporator water mass flow rate of 0.33 kg·s$^{-1}$, and ten different configurations, corresponding to those represented in Fig. 1.

The results presented in Fig. 5 are in good agreement with those presented by other researchers. The maximum COP for Conf. E is 3.16, which is slightly lower than the results obtained by Dai et al. [24], who reported a COP of around 3.4 during hot water generation at 40/45 °C and ambient temperature of 15 °C using what they called DDMS, which is similar to Conf. E. For the same operating conditions, the maximum COP obtained for Conf. B is 3.18, which is also slightly lower than the COP of 3.4 reported by He et al. [28] using what they called $BS_{WFC}$, which is almost the same configuration as Conf. B. In He et al. [28] $BS_{WFC}$ system, the water flows first through the condenser of the R1234yf cycle and then through the gas cooler of the $CO_2$ cycle, whereas in Conf. B the order is the opposite. When the water flows first through the condenser of the auxiliary cycle, there is a decrease in the subcooling effect, which affects negatively the main $CO_2$ cycle, but also a reduction in the condensation temperature that affects positively the auxiliary R1234yf cycle. According to the results obtained for Conf. C&C* and Conf. D&D*, it seems that globally, this effect has very little influence on the overall COP of the system and does not explain the deviation between the results obtained by previous researchers and those presented in Fig. 5; that deviation could be related to the differences in the models used for the compressors or the heat exchangers.

When the DMS is combined with an IHX, the efficiency of the system improves, although that improvement only is important when the $CO_2$ passes first through the IHX and then through the evaporator of the DMS cycle (Conf. D&D*). When the order is reversed (Conf. C&C*) the results are similar to those obtained without IHX (Conf. B), although the efficiency improves at low gas cooler pressure (below optimal pressure). Despite He et al. [28] reported a slight improvement in the COP when the water flow is divided (what they called $P_{WFC}$), the results obtained for Conf. E are almost exactly the same as those obtained for Conf. B, and the results for Conf. E* are similar or even slightly worse than those of Conf. D and Conf. D*.

Another important aspect that must be taken into account is that although both, Dai et al. [24], and He et al. [28] reported that the use of a DMS system improves the efficiency of the base cycle, they compare their improved DMS cycles to base cycles that do not include any subcooling method. According to the results presented in Fig. 5, when a cycle including a DMS system is compared to a base cycle that includes an IHX as a subcooling method, in most cases the DMS is not able to improve the efficiency of the base cycle. Only an indirect DMS system (Conf. F) is capable to improve the efficiency of the base cycle (Conf. A) without the necessity of including an additional subcooling method, showing an improvement of 15% in COP and 168% in heating capacity, and a decrease of 6 bar in the optimum gas cooler pressure. When this system is combined with an IHX as an additional subcooling method (Conf. F*, not studied previously by other authors) the efficiency improves (26% increase compared to Conf. A; almost 8.5% increase compared to Conf. F) while the heating capacity remains almost constant (163% increase compared to Conf. A, less than 2% decrease compared to Conf. F), and the optimum gas cooler pressure decreases (8 bar lower than Conf. A, 2 bar lower than Conf. F).

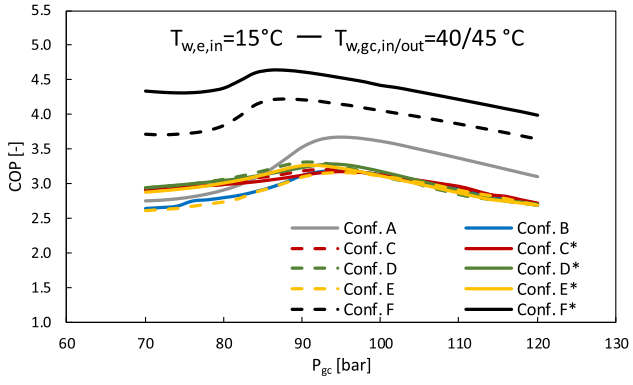


**Fig. 5.** COP vs gas cooler pressure for the ten configurations considered during intermediate temperature hot water generation and a fixed water temperature of 15 °C at the inlet of the evaporator.

Fig. 6 helps to better understand the differences among the configurations studied.

Fig. 6a shows the *T*-s diagram of Conf. A, which corresponds to a typical transcritical $CO_2$ cycle with IHX. The high-pressure $CO_2$ that leaves the gas cooler at point $3_{CO2}$ enters the IHX and lowers its temperature until it reaches point $4_{CO2}$, while exchanging heat with the low-pressure $CO_2$ that exits from the evaporator at point $6_{CO2}$ and is heated until it reaches point $1_{CO2}$. For this configuration, the water is heated up exclusively in the gas cooler, and the compressor power input represents the only energy consumption of the system.

Fig. 6b shows the *T*-s diagram of Conf. B, corresponding to a transcritical $CO_2$ cycle with DMS and without IHX. In this case, the $CO_2$ leaving the gas cooler at point $3_{CO2}$ enters the DMS evaporator where it is cooled until it reaches point $4_{CO2}$. The water is heated up in both, the gas cooler of the main cycle, and the condenser of the DMS cycle, and the energy consumption is the sum of the power absorbed by the $CO_2$ and the DMS compressors. As can be deduced from the results presented in Table 3, the heat transfer rate in the evaporator for Conf. B is clearly higher than for Conf. A, which leads to a lower evaporation temperature. Since the optimal gas cooler pressure is the same for Conf. A and Conf. B (see Fig. 5 and Table 3), and the evaporation temperature is lower for Conf. B, both the compressor isentropic efficiency and the COP of the main $CO_2$ cycle are lower for Conf. B. Given that the evaporation temperature of the DMS cycle is also relatively low, the COP of the DMS cycle does not compensate for the low COP of the main $CO_2$ cycle, leading to a lower overall COP for the whole system.

Fig. 6c shows the *T*-s diagram of Conf. C, which corresponds to a transcritical $CO_2$ cycle with DMS and with an IHX located after the DMS evaporator. As Fig. 6c shows, for the operating conditions represented, the temperature of the $CO_2$ leaving the evaporator of the DMS cycle at point $4_{CO2}$ is only slightly higher than the temperature of the $CO_2$ leaving the evaporator of the main $CO_2$ cycle at point $7_{CO2}$. Therefore, in this configuration the IHX has very little impact on the efficiency of the system and the overall efficiency of the system is almost the same as for Conf. B. The *T*-s diagram of Conf. C*, not included in Fig. 6, is very similar, with a higher gas cooler pressure and a lower DMS condenser pressure.

Fig. 6d shows the *T*-s diagram of Conf. D, which corresponds to a transcritical $CO_2$ cycle with DMS and with an IHX located before the DMS evaporator. Since the $CO_2$ enters the IHX as soon as it leaves the gas cooler, the enthalpy change in the IHX is similar to that of Conf. A. On the other hand, since the $CO_2$ enters the evaporator of the DMS cycle at a lower temperature, the subcooling effect in the DMS evaporator is slightly lower than that of Conf. B and the evaporation temperature of the DMS cycle is also lower. Nevertheless, the subcooling effect in the DMS evaporator is around three times the subcooling effect in the IHX. Similarly to what happens in Conf. B and Conf. C, the enthalpy of the $CO_2$ that enters the evaporator of the main cycle is very low, leading to a

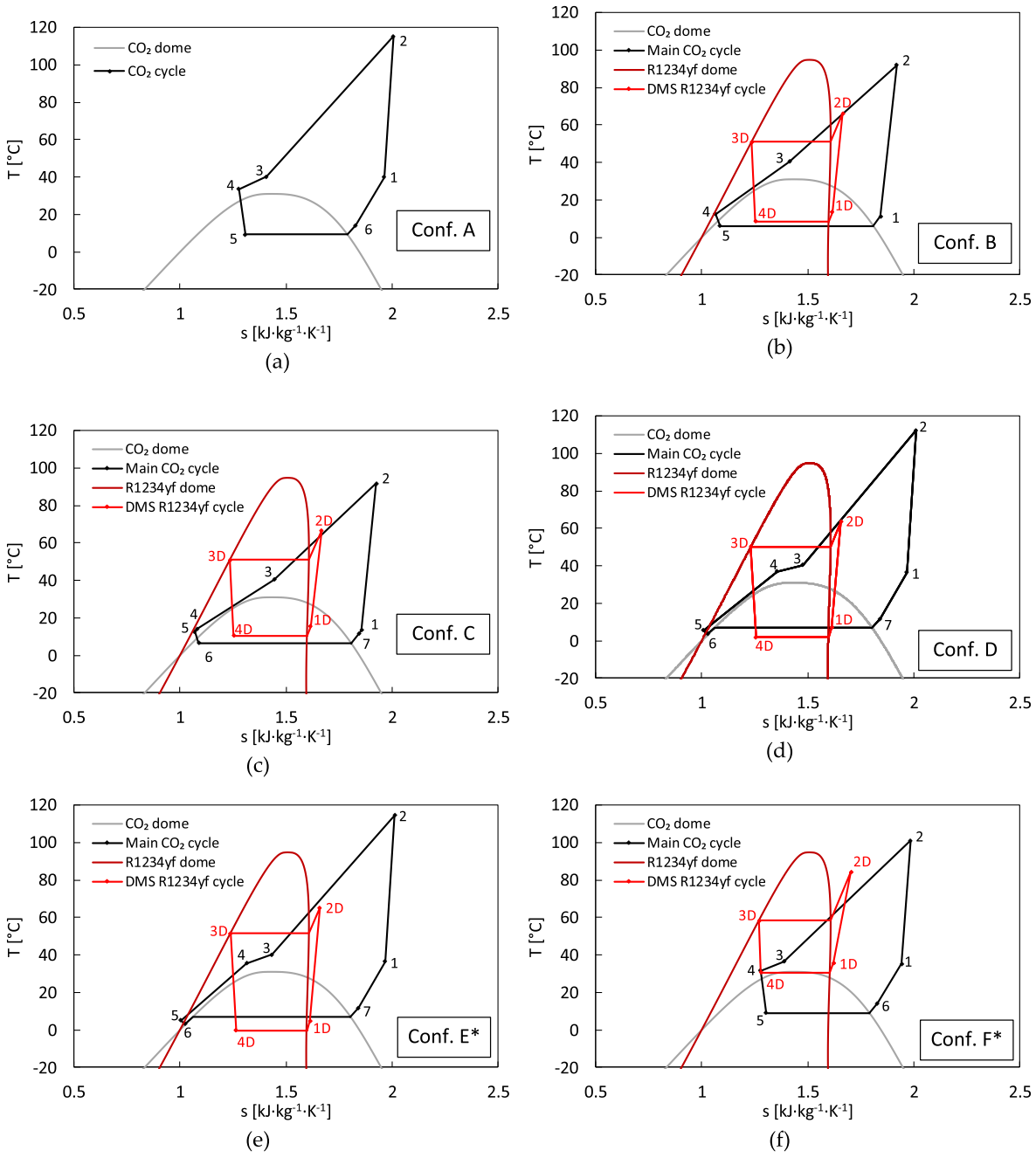


**Fig. 6.** Temperature-entropy diagrams for some of the configurations studied at hot water inlet/outlet temperature of 40/45 °C, fixed water temperature of 15 °C at the inlet of the evaporator, and optimal gas cooler pressure.

lower evaporation temperature and a lower COP of the main cycle. Consequently, the overall COP although better than for Conf. B and Conf. C is still worse than for Conf. A. The *T*-s diagram of Conf. D*, not included in Fig. 6, is very similar, with a higher gas cooler pressure and a lower DMS condenser pressure.

Fig. 6e corresponds to Conf. E* and, as it can be seen, the *T*-s diagram is very similar to that of Conf. D. The only difference between Conf. D and Conf. E* is that the water flow is divided into two streams, half of the flow goes to the gas cooler of the main cycle and the other half goes to the condenser of the DMS cycle. Despite the water entering at a lower temperature, the condensation temperature of the DMS cycle is slightly higher than for Conf. D due to the lower water flowrate. On the whole, the difference between both configurations is very little, and, as well as the *T*-s diagram, the COP is also very similar. The *T*-s diagram of Conf. E, not included in Fig. 6, is very similar to that corresponding to Conf. B.

Fig. 6f shows the *T*-s diagram of Conf. F*, corresponding to a transcritical $CO_2$ cycle with IHX and indirect DMS. The *T*-s diagram of the main $CO_2$ cycle is very similar to that of Conf. A, in fact, the evaporation temperature is almost the same but, since the water enters the gas cooler at a lower temperature because of the cooling in the evaporator of the DMS cycle, the temperature of the $CO_2$ leaving the gas cooler is lower, and therefore the optimal gas cooler pressure is clearly lower than in Conf. A and, consequently, the COP of the main $CO_2$ cycle is higher than in Conf. A. On the other hand, the *T*-s diagram of the DMS cycle is very different from all the other configurations. Since the water that is going to be heated up enters both, the evaporator and the condenser of the DMS cycle, the evaporation temperature of that cycle is clearly higher than in the rest of the configurations. Although the condensation temperature also increases due to the increase in the evaporation temperature, that increase is less accentuated and therefore the COP of the DMS

**Table 3**
Influence of the configuration at maximum COP gas cooler pressure and 15 °C evaporator water inlet temperature.

| | $T_{w,gc,in/out}$ | Conf. A | Conf. B | Conf. C | Conf. C* | Conf. D | Conf. D* | Conf. E | Conf. E* | Conf. F | Conf. F* |
|---|---|---|---|---|---|---|---|---|---|---|---|
| $\dot{Q}_t$ | | | | | | | | | | | |
| (kW) | 10/60 °C | 7.68 | 9.52 | 9.74 | 10.26 | 10.17 | 9.01 | 10.00 | 9.39 | | |
| | 30/60 °C | 5.61 | 10.02 | 9.99 | 9.83 | 9.23 | 8.44 | 10.09 | 8.84 | 12.76 | 12.81 |
| | 50/60 °C | 4.84 | 10.25 | 9.62 | 9.27 | 8.17 | 8.04 | 10.21 | 8.18 | 13.90 | 13.79 |
| | 40/45 °C | 5.17 | 10.14 | 9.84 | 10.08 | 8.58 | 8.53 | 10.15 | 8.68 | 13.85 | 13.59 |
| $p_{gc}$ | | | | | | | | | | | |
| (bar) | 10/60 °C | 70 | 70 | 70 | 80 | 70 | 80 | 78 | 72 | | |
| | 30/60 °C | 84 | 78 | 78 | 94 | 78 | 98 | 88 | 86 | 70 | 70 |
| | 50/60 °C | 110 | 108 | 104 | 102 | 100 | 104 | 108 | 100 | 100 | 98 |
| | 40/45 °C | 94 | 94 | 92 | 96 | 90 | 94 | 94 | 92 | 88 | 86 |
| $\dot{Q}_{gc}$ | | | | | | | | | | | |
| (%) | 10/60 °C | 100.00 | 83.72 | 83.11 | 59.67 | 80.48 | 73.51 | 68.27 | 67.62 | | |
| | 30/60 °C | 100.00 | 56.95 | 57.07 | 51.23 | 61.74 | 63.03 | 0.00 | 61.64 | 55.36 | 55.21 |
| | 50/60 °C | 100.00 | 48.96 | 45.68 | 39.02 | 49.76 | 47.79 | 47.64 | 49.74 | 36.91 | 35.86 |
| | 40/45 °C | 100.00 | 53.82 | 51.81 | 52.49 | 55.17 | 56.68 | 53.99 | 58.97 | 39.60 | 38.15 |
| COP | | | | | | | | | | | |
| (-) | 10/60 °C | 6.08 | 3.87 | 3.96 | 4.02 | 3.96 | 4.30 | 4.34 | 4.63 | | |
| | 30/60 °C | 4.40 | 3.38 | 3.39 | 3.23 | 3.46 | 3.30 | 3.50 | 3.63 | 5.20 | 5.31 |
| | 50/60 °C | 2.92 | 2.50 | 2.57 | 2.58 | 2.65 | 2.66 | 2.55 | 2.73 | 3.39 | 3.84 |
| | 40/45 °C | 3.66 | 3.18 | 3.20 | 3.17 | 3.32 | 3.29 | 3.16 | 3.27 | 4.22 | 4.64 |

cycle is clearly better than in the rest of the configurations studied. In short, Conf. F* combines the higher COP for both, the main $CO_2$ cycle and the DMS cycle and therefore, the overall COP is the highest of all configurations studied. The *T*-s diagram of Conf. F, not included in Fig. 6, is similar but it includes neither the subcooling from point $3_{CO2}$ to point $4_{CO2}$ nor the superheating from point $6_{CO2}$ to point $1_{CO2}$.

Fig. 7 is similar to Fig. 5, but changes the heated water inlet/outlet temperature. The results presented correspond to three different stages during domestic hot water (DHW) generation and a fixed water temperature of 15 °C at the inlet of the evaporator. The conclusions that can be drawn are similar to those obtained from Fig. 5, that is, the use of a DMS system only improves the efficiency of the base IHX system for Conf. F and Conf. F*. In fact, according to Fig. 8, it seems that there is a transition temperature around 22 °C above which Conf. F* is more efficient than Conf. A, whereas below 22 °C Conf. A is more efficient. When a DMS system is indirectly coupled to a main transcritical $CO_2$ system (Conf. F*), the water that enters the system passes through the evaporator of the DMS cycle before entering the gas cooler. Therefore, as Fig. 8 shows, the temperature of the water that enters the gas cooler decreases, the optimum gas cooler pressure decreases, and the efficiency of the main $CO_2$ system increases (COP ($CO_2$) is always higher than COP (A) in Fig. 8). On the other hand, since the efficiency of the DMS system is lower than the efficiency of the main $CO_2$ system, the efficiency of the whole system is lowered. In fact, when the water enters the system below 22 °C, the improvement in the efficiency of the main $CO_2$ cycle does not compensate for the low efficiency of the DMS system and the COP of the whole system using Conf. F* is lower than the COP of Conf. A. Therefore, during the first stages of DHW generation, the compressor of the DMS system should remain off until the water temperature reaches a value around 22 °C, and the three-way valves 3WV-1, and 3WV-2 (Fig. 1f) should be operated to send all the water to the gas cooler while bypassing the evaporator of the DMS cycle.

The results for Conf. F&F* are not plotted in Fig. 7a because, in order to increase the water temperature from 10 °C to 60 °C, the water mass flow rate has to be very low. In those conditions, the evaporation temperature in the DMS cycle is lower than the minimum evaporation temperature allowed in the code to avoid the freezing of the secondary fluid. Similarly, some cases are not plotted in Fig. 7b because the solutions found by the code violate the restrictions imposed (for example, the difference between the water temperature at the condenser/gas cooler outlet and the refrigerant at the compressor outlet is lower than the minimum allowed value).

The results presented in Fig. 5 and Fig. 7 for the efficiency are summarized in Table 3, along with the results obtained for the total heating capacity and the percentage of the total capacity supplied by the gas cooler of the main $CO_2$ cycle. Taking as reference the results for the system water inlet/outlet temperatures of 40/45 °C, although the basic transcritical $CO_2$ cycle with IHX and without DMS provides better efficiency than all direct DMS cycles (COP of 3.66 for Conf. A; COP from 3.16 to 3.32 for Conf. B to Conf. E*), the total heating capacity is clearly lower (5.17 kW for Conf. A; between 8.53 kW and 10.15 kW for Conf. B to Conf. E*). On the other hand, indirect DMS systems (Conf. F and Conf. F*) not only provide higher heating capacity (13.85 kW and 13.59 kW respectively; 168% and 163% increase), but also better efficiency (COP of 4.22 and 4.64; 15% and 27% improvement).

Fig. 9 summarizes the variation in the total capacity, the COP, and the optimum gas cooler pressure (in parts per unit) compared to the base cycle (Conf. A) for all configurations studied.

### 4.2. Influence of the auxiliary compressor capacity

A key aspect to maximize the efficiency of a transcritical $CO_2$ heat pump with DMS is to find the optimum subcooling degree that, in most cases, has not been quantified [6]. The subcooling degree achieved using a DMS system is directly related to the cooling capacity of the DMS system, which mainly depends on the refrigerant mass flow rate delivered by its compressor.

The influence that the capacity of the auxiliary compressor has on the efficiency of the system has been investigated by varying the compressor speed. The compressor available in the experimental facility and simulated in this work is not a variable speed compressor, and the manufacturer's software only provides its performance at nominal speed, whereas, for variable speed compressors, the software provides performance curves in the form:

$$\begin{aligned} x = {} & C_1 + C_2\hat{A}\cdot T_e + C_3\hat{A}\cdot T_c + C_4\hat{A}\cdot v + C_5\hat{A}\cdot T_e\hat{A}\cdot T_c + C_6\hat{A}\cdot T_e\hat{A}\cdot v \\ & + C_7\hat{A}\cdot T_c\hat{A}\cdot v + C_8\hat{A}\cdot T_e^2 + C_9\hat{A}\cdot T_c^2 + C_{10}\hat{A}\cdot v^2 + C_{11}\hat{A}\cdot T_e\hat{A}\cdot T_c\hat{A}\cdot v \\ & + C_{12}\hat{A}\cdot T_e^2\hat{A}\cdot T_c + C_{13}\hat{A}\cdot T_e^2\hat{A}\cdot v + C_{14}\hat{A}\cdot T_e^3 + C_{15}\hat{A}\cdot T_e\hat{A}\cdot T_c^2 \\ & + C_{16}\hat{A}\cdot T_c^2\hat{A}\cdot v + C_{17}\hat{A}\cdot T_c^3 + C_{18}\hat{A}\cdot T_e\hat{A}\cdot v^2 + C_{19}\hat{A}\cdot T_c\hat{A}\cdot v^2 + C_{20}\hat{A}\cdot v^3 \end{aligned} \quad (6)$$

where $x$ is the dependent variable (cooling capacity, $\dot{Q}_e$, or power input, $\dot{W}_r$), $T_e$ and $T_c$ are the evaporation and condensation temperatures (in °C), $v$ is the compressor speed (in rpm), and the adjustment coefficients, $C_i$, depend on the variable considered and can be obtained from Copeland Select 8 Software.

In order to simulate the efficiency of the system when the compressor speed varies, a variable speed compressor of similar nominal displace-

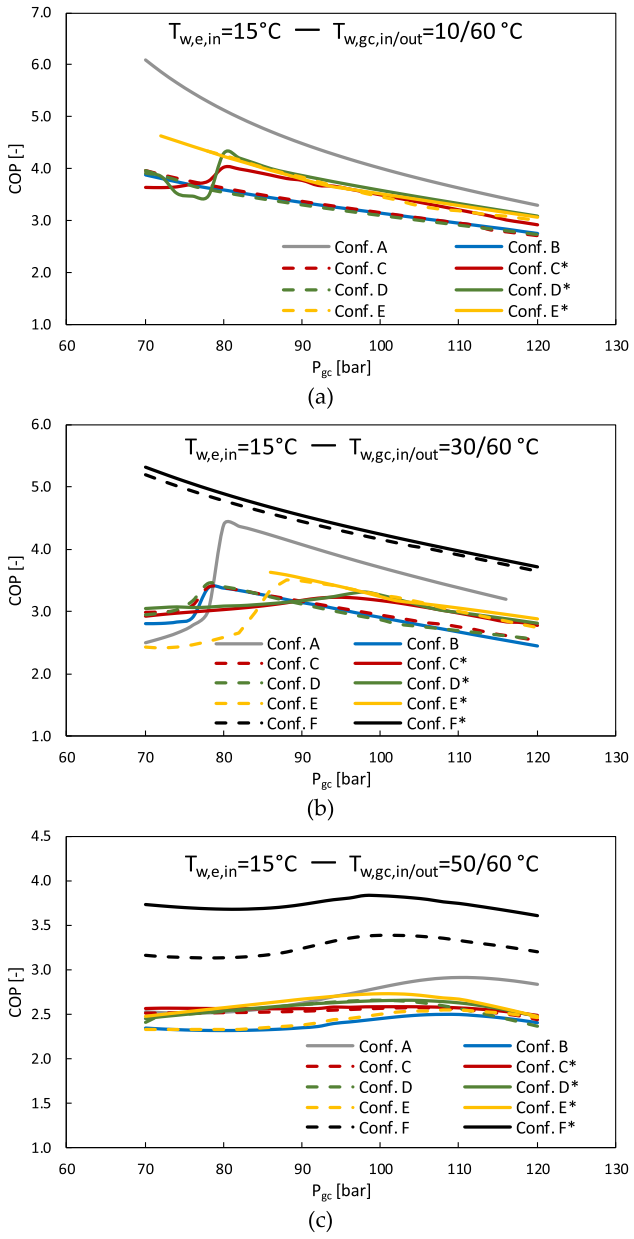


**Fig. 7.** COP vs gas cooler pressure for the ten configurations considered for three different stages during DHW generation and a fixed water temperature of 15 °C at the inlet of the evaporator.

ment has been selected (Copeland ZHW0302; $\dot{V} = 5.3 m^3 \cdot h^{-1}$). Then, its mass flow rate (obtained from the cooling capacity) and power input has been calculated for eleven different compressor speeds (from 900 to 6900 rpm), seven different evaporation temperatures (from −10 to 20 °C), and seven condensation temperatures (from 30 to 60 °C). Using those data, mass flow rate and power input modifier curves have been obtained. Those curves are normalized to 1 at nominal compressor speed (3600 rpm). The output of those curves is multiplied by the mass flow rate (or power input) to give the mass flow rate (or power input) at a specific compressor speed. The results obtained from that procedure are the modifier curves for the mass flow rate ($F_1$), and the power input ($F_2$):

$$F_1 = -0.05639904 - 0.000176344 \cdot T_e - 0.000156035 \cdot T_c + 0.000294627 \cdot v \quad (7)$$

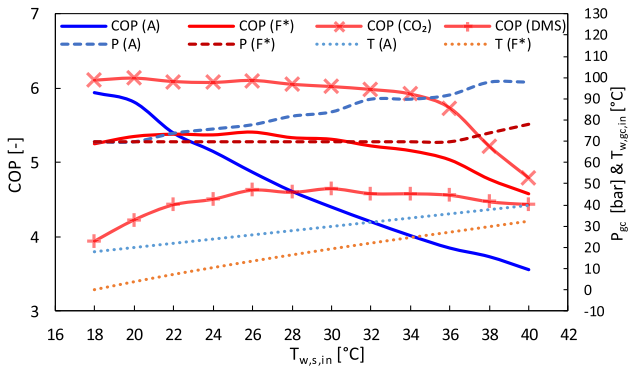


**Fig. 8.** COP, gas cooler pressure ($p_{gc}$) and temperature of the water that enters the gas cooler ($T_{w.gc,in}$) against the temperature of the water that enters the system ($T_{w.s,in}$) for Conf. A and Conf. F* at a fixed water temperature of 15 °C at the inlet of the evaporator.

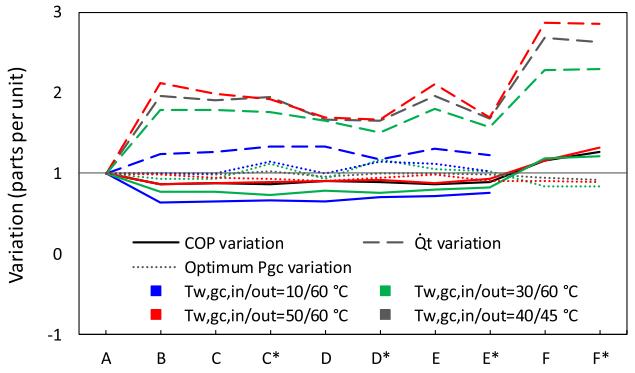


**Fig. 9.** COP and total heating capacity variation respect to the base cycle (Conf. A) for all configurations studied.

$$F_2 = 0.030315003 + 0.001376794 \cdot T_e - 0.002322145 \cdot T_c + 0.000306503 \cdot v \quad (8)$$

where the coefficient of determination is $R^2 = 0.9997$ for $F_1$, and $R^2 = 0.9962$ for $F_2$.

The same modifier curves have been assumed to be applicable to the compressor simulated, assuming the same speed operation range (900–7020 rpm). Therefore, the final model adopted for the R1234yf compressor is:

$$\dot{m}_r = F_1 \cdot \left[C_1 + C_2 \cdot T_e + C_3 \cdot T_c + C_4 \cdot T_e^2 + C_5 \cdot T_e \cdot T_c + C_6 \cdot T_c^2 + C_7 \cdot T_e^3 + C_8 \cdot T_c \cdot T_e^2 + C_9 \cdot T_e \cdot T_c^2 + C_{10} \cdot T_c^3\right] \quad (9)$$

$$\dot{W}_r = F_2 \cdot \left[D_1 + D_2 \cdot T_e + D_3 \cdot T_c + D_4 \cdot T_e^2 + D_5 \cdot T_e \cdot T_c + D_6 \cdot T_c^2 + D_7 \cdot T_e^3 + D_8 \cdot T_c \cdot T_e^2 + D_9 \cdot T_e \cdot T_c^2 + D_{10} \cdot T_c^3\right] \quad (10)$$

Fig. 10 shows the results obtained using this model to analyze the influence of the auxiliary compressor speed for two different water flow configurations (Conf. E* and Conf. F*). According to the results presented, the influence of the compressor speed (and therefore, the compressor cooling capacity) is strongly dependent on the water flow configuration.

The results for Conf. E* show that the maximum COP is obtained for the lower compressor speed, which is in good agreement with what Nebot-Andrés et al. [48] found in a similar configuration, although operating as a refrigeration plant. Although the maximum efficiency is obtained for the minimum speed (900 rpm), the difference with the next speed simulated (1500 rpm) is lower than among the other speeds

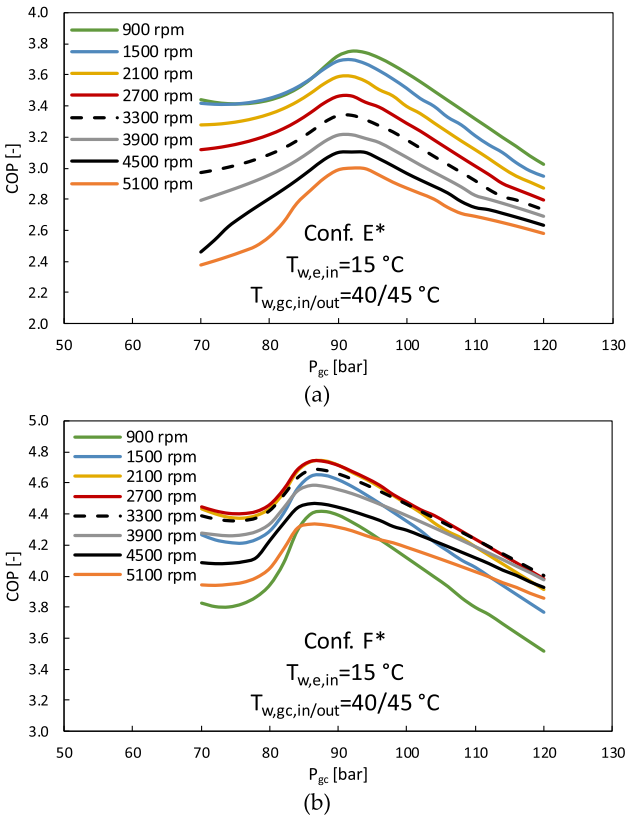


**Fig. 10.** Influence of the compressor speed during intermediate temperature hot water generation and a fixed water temperature of 15 °C at the inlet of the evaporator.

simulated, and the optimum gas cooler pressure increases, so it seems that even if the speed could be lower, the optimum value should be around 900 rpm.

According to other results provided by the model and not included in the figures presented, a variation in the auxiliary compressor speed affects mainly the evaporation pressure of the DMS cycle, which clearly increases as the speed decreases. There is also a decrease in the condensation temperature, but much weaker than the increase in the evaporation temperature. Finally, as the compressor speed increases, the cooling capacity of the auxiliary cycle increases, and thus the enthalpy at the inlet of the main evaporator decreases, producing a slight decrease in the evaporation temperature of the main cycle that worsens its efficiency. Therefore, a decrease in the compressor speed produces a strong improvement in the auxiliary cycle efficiency and a slight improvement in the main cycle efficiency, improving the overall efficiency, although decreasing the total heating capacity.

The results for Conf. F* are clearly different. It seems that there is an optimum speed around 2700 rpm, although low increases or decreases around that value have little impact on the overall efficiency. Below 2100 rpm, and over 3300 rpm, the efficiency clearly decreases. Therefore, using this configuration, the optimum auxiliary compressor capacity is similar to the actual capacity of the compressor simulated and, in fact, the heating capacity of the auxiliary cycle represents around 55% of the total heating capacity of the system. On the other hand, in Conf. E* the auxiliary compressor should be clearly smaller in order to optimize the overall efficiency and the heating capacity of the auxiliary cycle represents only around 20% of the total heating capacity of the system.

The influence of a variation on the auxiliary compressor speed is clearly different for Conf. F*. Although associated with a decrease in the compressor speed, there is also an increase in the evaporation temperature and a decrease in the condensation temperature, the influence is inverted compared to Conf. E*. The change in the evaporation temperature is much weaker whereas the change in the condensation temperature is much stronger. There is a point in which the improvement in the auxiliary cycle operating conditions do not compensate for the decrease in the efficiency of the compressor and therefore the DMS cycle presents its optimum efficiency at 1500 rpm. Whereas the COP and the heating capacity of the main cycle are almost constant, in the auxiliary cycle both variables are strongly dependent on the compressor speed and, as a result, the optimum efficiency for the whole system is reached at a compressor speed higher than the optimum speed for the auxiliary cycle.

### 4.3. *Influence of the distribution of the water flow*

All results presented for Conf. E&E* and Conf. F&F* have been calculated assuming that the water mass flow rate sent to the gas cooler is the same as the mass flow rate sent to the auxiliary cycle condenser. Fig. 11 analyzes the influence that the distribution of the water mass flow rate has on the efficiency of the system, where the legend (X/Y) means X% of the total flow sent to the gas cooler, Y% sent to the condenser.

The results for Conf. E* show that when the water mass flow rate fraction sent to the gas cooler is around 35% of the total, the system reaches its maximum efficiency. The mass flow rate fraction has the opposite effect on the auxiliary and the main cycle. An increase of the fraction sent to the gas cooler implies a decrease of that sent to the condenser of the auxiliary cycle and produces an increase in the auxiliary cycle condensation temperature and a decrease in its evaporation temperature, worsening the efficiency of the auxiliary cycle. On the other hand, when the mass flow rate flowing through the gas cooler increases, the refrigerant temperature at the gas cooler outlet decreases, and the efficiency of the main cycle improves. For a mass flow rate fraction sent to the gas cooler of around 45%, the system reaches a point

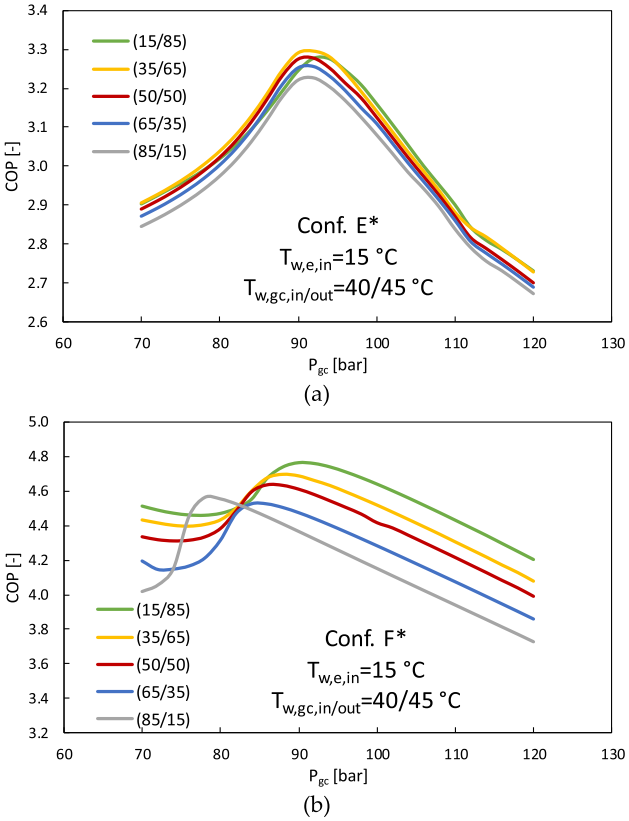


**Fig. 11.** Influence of the water mass flow rate fraction during intermediate temperature hot water generation and a fixed water temperature of 15 °C at the inlet of the evaporator.

in which the gas cooler is operating at its maximum efficiency, and an increase in the mass flow rate does not produce a decrease in the refrigerant outlet temperature. From this point, the efficiency of the main cycle remains constant. As a result, the system presents an optimum for a mass flow rate fraction of around 35%.

As Fig. 11 shows, when the system operates on Conf. F* the influence of the mass flow rate fraction is different. The lower the mass flow rate sent to the gas cooler of the main cycle, the highest the efficiency of the whole system. For this configuration, an increase in the fraction sent to the gas cooler implies an increase in the fraction sent to the auxiliary cycle evaporator, which has a beneficial effect on the auxiliary cycle COP, and a decrease in the fraction sent to the auxiliary cycle condenser, which has a negative effect on the auxiliary cycle COP. The increase in the condensation temperature is slightly higher than the decrease in the evaporation temperature and, additionally, it has a stronger impact on the compression rate. Consequently, an increase in the mass flow rate fraction flowing through the gas cooler produces an increase in the compression rate of the auxiliary cycle and a decrease in its efficiency. When the fraction sent to the gas cooler increases, the temperature of the water leaving the evaporator of the auxiliary cycle increases slightly, but this effect is compensated by the increase in the efficiency of the gas cooler and has very little impact on the temperature of the refrigerant leaving the gas cooler. As a result, the efficiency of the main cycle remains almost constant. Since the COP of the main cycle is almost constant and the COP of the auxiliary cycle clearly worsens, the COP of the whole system also decreases as the mass flow rate fraction sent to the gas cooler increases.

### 4.4. Influence of the main cycle evaporation temperature

Fig. 12 shows the influence that the temperature of the water entering the evaporator of the main cycle has on the efficiency of the whole system. As well as for all the results previously presented, results plotted in Fig. 12 were obtained for an evaporator water mass flow rate of 0.33 kg·s$^{-1}$.

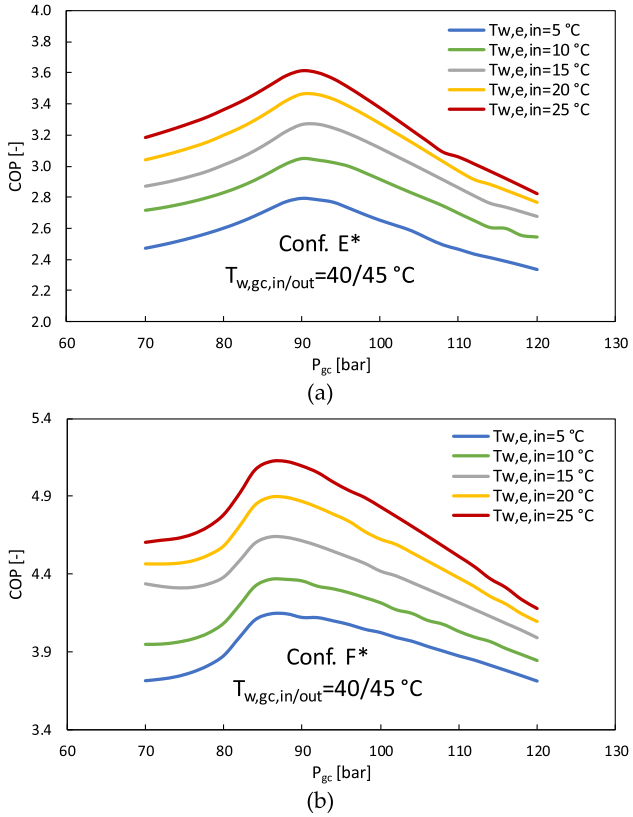


**Fig. 12.** Influence of the water temperature at the inlet of the evaporator.

As expected, an increase in the water temperature produces an improvement in the efficiency of the main cycle that has a positive effect on the efficiency of the whole system for both, Conf. E* and Conf. F*. It can be also noticed that, although not very important, the evaporation temperature has an impact on the optimal pressure of the gas cooler. As Fig. 12 shows, as the water temperature increases, the optimal gas cooler pressure increases too in both configurations.

## 5. Conclusions

This work explores different configurations of $CO_2$ transcritical heat pump cycles coupled to IHX and DMS for hot water generation. The numerical model is briefly described and then the results obtained at different operating conditions are presented and analyzed in order to compare their performance. Whereas most previous works compare their results to a base cycle that not use any subcooling method works, this study takes as base system for comparison a transcritical $CO_2$ system that already includes an IHX as subcooling system. This system has been chosen as base cycle because of its relatively low cost, its simplicity, and its proven capacity to improve the performance of transcritical $CO_2$ systems under very different operating conditions.

The numerical results show that the way in which the water is distributed among the main and the auxiliary cycle has an important influence on the efficiency of a $CO_2$ transcritical heat pump coupled to a DMS system. In fact, in most cases, the use of an IHX is preferred over a DMS system, and only when the coupling between both cycles is performed by the water flowing first through the evaporator of the auxiliary cycle and then through the gas cooler of the main cycle, there is an improvement in the efficiency. A new configuration, not studied previously by other researchers, which combines indirect DMS and IHX has been proposed as the best solution, combining the best efficiency with almost the highest heating capacity and the lowest gas cooler optimum pressure.

The main results can be summarized as follow:

- For all conditions simulated, the use of direct DMS systems, whether the DMS is the only subcooling method or it is combined with an IHX, produces an increase in the total heating capacity of the system, but a decrease in the overall efficiency, when compared to the base configuration of $CO_2$ cycle with IHX and without DMS.
- The use of indirect DMS systems (Conf. F & Conf. F*) provides an increase in both, the efficiency and the heating capacity, as well as a decrease in the optimum gas cooler pressure compared to the base configuration of $CO_2$ cycle with IHX and without DMS.
- Indirect DMS system without IHX (Conf. F) improves the efficiency of the base cycle by 16.5% on average, with an average increase of 160% in heating capacity and a reduction in the gas cooler optimum pressure.
- The performance of indirect DMS systems can be improved by including an IHX as an additional subcooling method (Conf. F*). The results obtained show, compared to the indirect system without IHX, an average increase of 8.5% in the COP, with similar heating capacity (average decrease lower than 1%) and even lower gas cooler optimum pressure (between 0 and 2 bar of reduction depending on the operating conditions studied).
- The use of indirect DMS systems is only recommended if the water to be heated enters the system at a temperature above 22 °C approximately; below that temperature, the base system with IHX and without DMS provides better efficiency. Therefore, in space heating applications, the indirect DMS system is always recommended, preferably with IHX (V1 closed, V2 and V3 opened in Fig. 1f; Conf. F*), whereas in DHW generation applications is recommended a system capable to switch between the base cycle and an indirect DMS system with IHX. That kind of system corresponds to the layout proposed in Fig. 1f, which allows switching between Conf. A and

Conf. F* by activating or deactivating the compressor and acting on the three-way valves represented in that figure.

- The influence that the size of the compressor used in the auxiliary cycle has on the efficiency of the whole system has been analyzed by varying the auxiliary compressor speed. The results show that this parameter has an important impact. Although the optimum compressor capacity depends on the configuration used, and for most configurations, the optimum efficiency is obtained when the capacity of the auxiliary compressor is lower than that of the main compressor, in the case of the best efficiency configuration (Conf. F*) the optimum efficiency is obtained when the capacity of the auxiliary compressor is similar or slightly lower than that of the main compressor (depending on the operating conditions, the percentage of the total heating capacity of the system generated in the condenser of the auxiliary cycle varies from 65% to 45%).
- In those configurations in which the water is divided into two different streams, the percentage of water sent to each heat exchanger also has an important influence on the efficiency of the system. Although this influence also depends on the configuration used, in general terms the optimum efficiency is obtained when the water flow is sent predominantly to the auxiliary cycle.

## Declaration of Competing Interest

The authors declare that they have no known competing financial interests or personal relationships that could have appeared to influence the work reported in this paper.

## Data availability

Data will be made available on request.

## Funding

This research was funded by the Spanish Ministry of Science and Innovation under Project TED2021-131173B-I00 and the NextGenerationEU recovery plan.

## References

[1] P. Nekså, H. Rekstad, G.R. Zakeri, P.A. Schiefloe, $CO_2$-heat pump water heater: Characteristics, system design and experimental results, Int. J. Refrig. 21 (1998) 172–179, https://doi.org/10.1016/S0140-7007(98)00017-6.

[2] L. Cecchinato, M. Corradi, E. Fornasieri, L. Zamboni, Carbon dioxide as refrigerant for tap water heat pumps: A comparison with the traditional solution, Int. J. Refrig. 28 (2005) 1250–1258, https://doi.org/10.1016/j.ijrefrig.2005.05.019.

[3] F. Illán-Gómez, V.F. Sena-Cuevas, J.R. García-Cascales, F.J.S. Velasco, Analysis of the optimal gas cooler pressure of a $CO_2$ heat pump with gas bypass for hot water generation, Appl. Therm. Eng. 182 (2021), 116110, https://doi.org/10.1016/j.applthermaleng.2020.116110.

[4] F. Illán-Gómez, V.F. Sena-Cuevas, J.R. García-Cascales, F.J.S. Velasco, Experimental and numerical study of a $CO_2$ water-to-water heat pump for hot water generation, Int. J. Refrig. 132 (2021) 30–44, https://doi.org/10.1016/j.ijrefrig.2021.09.020.

[5] S.M.H. Mohammadi, Theoretical investigation on performance improvement of a low-temperature transcritical carbon dioxide compression refrigeration system by means of an absorption chiller after-cooler, Appl. Therm. Eng. 138 (2018) 264–279, https://doi.org/10.1016/j.applthermaleng.2018.04.006.

[6] R. Llopis, L. Nebot-Andrés, D. Sánchez, J. Catalán-Gil, R. Cabello, Subcooling methods for $CO_2$ refrigeration cycles: A review, Int. J. Refrig. 93 (2018) 85–107, https://doi.org/10.1016/j.ijrefrig.2018.06.010.

[7] S.D. White, M.G. Yarrall, D.J. Cleland, R.A. Hedley, Modelling the performance of a transcritical $CO_2$ heat pump for high temperature heating, Int. J. Refrig. (2002) 479–486, https://doi.org/10.1016/S0140-7007(01)00021-4.

[8] S.G. Kim, Y.J. Kim, G. Lee, M.S. Kim, The performance of a transcritical $CO_2$ cycle with an internal heat exchanger for hot water heating, Int. J. Refrig. 28 (2005) 1064–1072, https://doi.org/10.1016/j.ijrefrig.2005.03.004.

[9] F.Z. Zhang, P.X. Jiang, Y.S. Lin, Y.W. Zhang, Efficiencies of subcritical and transcritical $CO_2$ inverse cycles with and without an internal heat exchanger, Appl. Therm. Eng. 31 (2011) 432–438, https://doi.org/10.1016/j.applthermaleng.2010.09.018.

[10] F. Cao, Y. Wang, Z. Ye, Theoretical analysis of internal heat exchanger in transcritical $CO_2$ heat pump systems and its experimental verification, Int. J. Refrig. 106 (2019) 506–516, https://doi.org/10.1016/j.ijrefrig.2019.05.022.

[11] Z. Ye, Y. Wang, Y. Song, X. Yin, F. Cao, Optimal discharge pressure in transcritical $CO_2$ heat pump water heater with internal heat exchanger based on pinch point analysis, Int. J. Refrig. 118 (2020) 12–20, https://doi.org/10.1016/j.ijrefrig.2020.06.003.

[12] E. Torrella, D. Sánchez, R. Llopis, R. Cabello, Energetic evaluation of an internal heat exchanger in a $CO_2$ transcritical refrigeration plant using experimental data, Int. J. Refrig. 34 (2011) 40–49, https://doi.org/10.1016/j.ijrefrig.2010.07.006.

[13] Y. Jiang, Y. Ma, M. Li, L. Fu, An experimental study of trans-critical $CO_2$ water-water heat pump using compact tube-in-tube heat exchangers, Energy Convers. Manage. 76 (2013) 92–100, https://doi.org/10.1016/j.enconman.2013.07.031.

[14] F. Cao, Z. Ye, Y. Wang, Experimental investigation on the influence of internal heat exchanger in a transcritical $CO_2$ heat pump water heater, Appl. Therm. Eng. 168 (2020), 114855, https://doi.org/10.1016/j.applthermaleng.2019.114855.

[15] D. Yang, Y. Song, F. Cao, L. Jin, X. Wang, Theoretical and experimental investigation of a combined R134a and transcritical $CO_2$ heat pump for space heating, Int. J. Refrig. 72 (2016) 156–170, https://doi.org/10.1016/j.ijrefrig.2016.07.016.

[16] Y. Song, D. Li, F. Cao, X. Wang, Investigation of the optimal intermediate water temperature in a combined r134a and transcritical $CO_2$ heat pump for space heating, Int. J. Refrig. 79 (2017) 10–24, https://doi.org/10.1016/j.ijrefrig.2017.04.018.

[17] Y. Song, Z. Ye, Y. Wang, F. Cao, The experimental verification on the optimal discharge pressure in a subcooler-based transcritical $CO_2$ system for space heating, Energy Build. 158 (2018) 1442–1449, https://doi.org/10.1016/j.enbuild.2017.11.015.

[18] Y. Song, F. Cao, The evaluation of the optimal medium temperature in a space heating used transcritical air-source $CO_2$ heat pump with an R134a subcooling device, Energy Convers. Manage. 166 (2018) 409–423, https://doi.org/10.1016/j.enconman.2018.04.052.

[19] Y. Song, F. Cao, The evaluation of optimal discharge pressure in a water-precooler-based transcritical $CO_2$ heat pump system, Appl. Therm. Eng. 131 (2018) 8–18, https://doi.org/10.1016/j.applthermaleng.2017.11.092.

[20] B. Dai, X. Zhao, S. Liu, Q. Yang, D. Zhong, Y. Cao, Y. Hao, Heating and cooling of residential annual application using DMS transcritical $CO_2$ reversible system and traditional solutions: An environment and economic feasibility analysis, Energy Convers. Manage. 210 (2020), 112714, https://doi.org/10.1016/j.enconman.2020.112714.

[21] B. Dai, X. Zhao, S. Liu, Q. Yang, D. Zhong, Y. Hao, Y. Hao, Energetic, exergetic and exergoeconomic assessment of transcritical $CO_2$ reversible system combined with dedicated mechanical subcooling (DMS) for residential heating and cooling, Energy Convers. Manage. 209 (2020), 112594, https://doi.org/10.1016/j.enconman.2020.112594.

[22] B. Dai, H. Qi, S. Liu, M. Ma, Z. Zhong, H. Li, M. Song, Z. Sun, Evaluation of transcritical $CO_2$ heat pump system integrated with mechanical subcooling by utilizing energy, exergy and economic methodologies for residential heating, Energy Convers. Manage. 192 (2019) 202–220, https://doi.org/10.1016/j.enconman.2019.03.094.

[23] B. Dai, H. Qi, S. Liu, Z. Zhong, H. Li, M. Song, M. Ma, Z. Sun, Environmental and economical analyses of transcritical $CO_2$ heat pump combined with direct dedicated mechanical subcooling (DMS) for space heating in China, Energy Convers. Manage. 198 (2019), 111317, https://doi.org/10.1016/j.enconman.2019.01.119.

[24] B. Dai, H. Qi, W. Dou, S. Liu, D. Zhong, H. Yang, V. Nian, Y. Hao, Life cycle energy, emissions and cost evaluation of $CO_2$ air source heat pump system to replace traditional heating methods for residential heating in China: System configurations, Energy Convers. Manage. 218 (2020), 112954, https://doi.org/10.1016/j.enconman.2020.112954.

[25] B. Dai, S. Liu, H. Li, Z. Sun, M. Song, Q. Yang, Y. Ma, Energetic performance of transcritical $CO_2$ refrigeration cycles with mechanical subcooling using zeotropic mixture as refrigerant, Energy. 150 (2018) 205–221, https://doi.org/10.1016/j.energy.2018.02.111.

[26] S. Liu, F. Lu, B. Dai, V. Nian, H. Li, H. Qi, J. Li, Performance analysis of two-stage compression transcritical $CO_2$ refrigeration system with R290 mechanical subcooling unit, Energy. 189 (2019), 116143, https://doi.org/10.1016/j.energy.2019.116143.

[27] J.-H. Cheng, Y.-J. He, C.-L. Zhang, New scenario of $CO_2$ heat pump for space heating: Automatic mode switch between modified transcritical and cascade cycle in one system, Appl. Therm. Eng. 191 (2021), 116864, https://doi.org/10.1016/j.applthermaleng.2021.116864.

[28] Y.-J. He, J.-H. Cheng, M.-M. Chang, C.-L. Zhang, Modified transcritical $CO_2$ heat pump system with new water flow configuration for residential space heating, Energy Convers. Manage. 230 (2021), 113791, https://doi.org/10.1016/j.enconman.2020.113791.

[29] Á. Casi, P. Aranguren, M. Araiz, D. Sanchez, R. Cabello, D. Astrain, Experimental evaluation of a transcritical $CO_2$ refrigeration facility working with an internal heat exchanger and a thermoelectric subcooler: Performance assessment and comparative, Int. J. Refrig. 141 (2022) 66–75, https://doi.org/10.1016/j.ijrefrig.2022.05.024.

[30] M. Karampour, S. Sawalha, Investigation of using Internal Heat Exchangers in $CO_2$ Trans-critical Booster System, in: Hu, W Zhao, G (ed.), 11th IIR Gustav Lorentzen Conference on Natural Refrigerants (2014): Natural Refrigerants and Environmental Protection (Pp. 453-460). Int. Inst. Refrigeration.

[31] D. Sánchez, J. Patiño, R. Llopis, R. Cabello, E. Torrella, F.V. Fuentes, New positions for an internal heat exchanger in a CO2 supercritical refrigeration plant. Experimental analysis and energetic evaluation, Appl. Therm. Eng. 63 (2014) 129–139, https://doi.org/10.1016/j.applthermaleng.2013.10.061.

[32] F.J.S. Velasco, M.R. Haddouche, F. Illán-Gómez, J.R. García-Cascales, Experimental characterization of the coupling and heating performance of a $CO_2$ water-to-water heat pump and a water storage tank for domestic hot water production system, Energy Build. 265 (2022), 112085, https://doi.org/10.1016/j.enbuild.2022.112085.
[33] R.A. Otón-Martínez, F. Illán-Gómez, J.R. García-Cascales, F.J.S. Velasco, M. Reda Haddouche, Impact of an internal heat exchanger on a transcritical $CO_2$ heat pump under optimal pressure conditions, Appl. Therm. Eng. 215 (2022), 118991, https://doi.org/10.1016/j.applthermaleng.2022.118991.
[34] G.-B. Wang, X.-R. Zhang, Thermoeconomic optimization and comparison of the simple single-stage transcritical carbon dioxide vapor compression cycle with different subcooling methods for district heating and cooling, Energy Convers. Manage. 185 (2019) 740–757, https://doi.org/10.1016/j.enconman.2019.02.024.
[35] ANSI/AHRI, Standard for performance rating of positive displacement refrigerant compressors and compressor units, ANSI/AHRI. 540 (2015) 1–19.
[36] Dorin software, (2022). http://www.dorin.com/en/Software/ (accessed March 5, 2020).
[37] CEN, EN 12900. Refrigerant compressors. Rating conditions, tolerances and presentation of manufacturer's performance data, (2013) 16.
[38] A.E. Dabiri, C.K. Rice, Compressor-simulation model with corrections for the level of suction gas superheat., ASHRAE Transactions. 87, Part 2 (1981) 771–782.
[39] Copeland Select 8, (2022). https://climate.emerson.com/en-gb/tools-resources/copeland-select-software.
[40] IMST-ART. A simulation tool to assist the selection, design and optimization of refrigeration equipment and components, (2021). hhttp://www.imst-art.com/.
[41] J.M. Corberán, I.O. Martínez, J. Gonzálvez, Charge optimisation study of a reversible water-to-water propane heat pump, Int. J. Refrig 31 (2008) 716–726, https://doi.org/10.1016/j.ijrefrig.2007.12.011.
[42] F. Botticella, L. Viscito, Seasonal Performance Analysis of a Residential Heat Pump Using Different Fluids with Low Environmental Impact, Energy Procedia 82 (2015) 878–885, https://doi.org/10.1016/j.egypro.2015.11.832.
[43] F. Correa, C. Cuevas, Air-water heat pump modelling for residential heating and domestic hot water in Chile, Appl. Therm. Eng. 143 (2018) 594–606, https://doi.org/10.1016/j.applthermaleng.2018.07.130.
[44] P. Catrini, A. Piacentino, F. Cardona, G. Ciulla, Exergoeconomic analysis as support in decision-making for the design and operation of multiple chiller systems in air conditioning applications, Energy Convers. Manage. 220 (2020), 113051, https://doi.org/10.1016/j.enconman.2020.113051.
[45] A.S. Utage, K.V. Mali, H.C. Phadake, Performance simulation of HFC-161 as an alternative refrigerant to HCFC-22 for room air conditioner, Mater. Today:. Proc. 47 (2021) 5594–5597, https://doi.org/10.1016/j.matpr.2021.03.474.
[46] F. Calise, F.L. Cappiello, L. Cimmino, M. Dentice d'Accadia, M. Vicidomini, Dynamic modelling and thermoeconomic analysis for the energy refurbishment of the Italian building sector: Case study for the "Superbonus 110%" funding strategy, Appl. Therm. Eng. 213 (2022), 118689, https://doi.org/10.1016/j.applthermaleng.2022.118689.
[47] CEN/TC 113, EN 14511-2. Air conditioners, liquid chilling packages and heat pumps for space heating and cooling and process chillers, with electrically driven compressors. Part 2: Test conditions, (2018) 20. https://standards.cen.eu/dyn/www/f?p=204:110:0:::FSP_PROJECT,FSP_ORG_ID:59177,6095&cs=109421BB169D17E8F2FB71B2B6025CA37.
[48] L. Nebot-Andrés, D. Calleja-Anta, D. Sánchez, R. Cabello, R. Llopis, Experimental assessment of dedicated and integrated mechanical subcooling systems vs parallel compression in transcritical $CO_2$ refrigeration plants, Energy Convers. Manage. 252 (2022), 115051, https://doi.org/10.1016/j.enconman.2021.115051.